Lobe cell convection and polar cap precipitation

S. Eriksson,[1] W. J. Peria,[2] J. W. Bonnell,[3] Y.-J. Su,[1] R. E. Ergun,[1] Y.-K. Tung,[3] G. K. Parks,[3] and C. W. Carlson[3]

Received 4 October 2002; revised 22 November 2002; accepted 7 January 2003; published 17 May 2003.

[1] The characteristic electric and magnetic field signature of lobe cells as observed by the low-altitude FAST satellite in 55 dawn-dusk passes are compared with Polar ultraviolet images of polar cap auroral activity. Initial results from 34 events of UV image coverage suggest that there is an intimate coupling between the sunward convection flow of the lobe cell and transpolar auroral arcs or diffuse polar cap precipitation in ~62% of these cases. However, in some cases where the field signatures are suggestive of lobe cell convection, there is no detectable particle precipitation either in Polar UVI or the FAST data sets. Moreover, the presence of lobe cells coincide with UV data intensifications in the premidnight 2000–2400 MLT sector and/or the postnoon 1500 MLT region in ~59% of all cases with UVI coverage. The magnetic local time dependence of the lobe cells and polar cap precipitation on the interplanetary magnetic field (IMF) are examined using the upstream Wind monitor. The relative importance of the IMF B_y and B_z components are investigated and compared with the predictions of the antiparallel merging model and strongly suggests a connection with the magnetospheric sash, as is further implied by the mapping of magnetic field lines using the *Tsyganenko* [2002] (T01) model. It was also noted that a majority of lobe cell events occurred during enhanced *AE* index substorm-like conditions and that generally stronger *AE* indices are measured for stronger IMF B_y magnitudes during these events. *INDEX TERMS:* 2760 Magnetospheric Physics: Plasma convection; 2776 Magnetospheric Physics: Polar cap phenomena; 2455 Ionosphere: Particle precipitation; 2431 Ionosphere: Ionosphere/magnetosphere interactions (2736); 2788 Magnetospheric Physics: Storms and substorms; *KEYWORDS:* plasma convection, polar cap phenomena, particle precipitation, solar wind/magnetosphere interactions, magnetosphere/ionosphere interactions

Citation: Eriksson, S., W. J. Peria, J. W. Bonnell, Y.-J. Su, R. E. Ergun, Y.-K. Tung, G. K. Parks, and C. W. Carlson, Lobe cell convection and polar cap precipitation, *J. Geophys. Res.*, *108*(A5), 1198, doi:10.1029/2002JA009725, 2003.

1. Introduction

[2] Lobe reconnection is a magnetospheric concept that has been around since the 1970s [*Russell*, 1972; *Crooker*, 1979]. It is based on the original idea of *Dungey* [1963] that the geomagnetic field of a completely closed model magnetosphere and the IMF become antiparallel and merge tailward of the cusp for a northward directed IMF. Later work have suggested that merging between the IMF and open tail lobe magnetic fields could drive sunward convection in the polar cap [e.g., *Crooker*, 1992], resulting in the so-called "lobe cells" on purely open field lines.

[3] The importance of the B_y component for lobe reconnection has been highlighted for a purely positive IMF B_y in magnetohydrodynamic (MHD) model studies by, e.g., *Crooker et al.* [1998] and *White et al.* [1998]. The former study concluded that the occurrence of lobe reconnection in the model and the presence of convection cells confined almost entirely to the polar cap (lobe cells) do not cease as the IMF turns southward and suggested that IMF B_x and B_y appear as more important controlling factors than IMF B_z. Moreover, the magnetosheath Alfvén Mach number, the ratio of the plasma flow speed to the Alfvén speed, seemed to control the relative strength of the model lobe cell circulation to the normal dayside two-cell convection pattern. The larger the Alfvén Mach number at the merging site, the weaker the lobe cell strength.

[4] Direct observations of lobe reconnection tailward of the cusp have so far been rare and was first reported in Hawkeye data by *Kessel et al.* [1996] for a predominantly northward IMF. Using ISEE-2 data, *Gosling et al.* [1991] had previously reported an observation on the Northern Hemispheric high-latitude dusk magnetopause, though for a predominantly duskward and antisunward IMF with a small southward IMF component. These examples support the so-called antiparallel model [*Crooker*, 1979; *Luhmann et al.*, 1984; *Crooker et al.*, 1998; *Rodger et al.*, 2000; *Raeder et*

[1]Laboratory for Atmospheric and Space Physics, University of Colorado, Boulder, Colorado, USA.
[2]Department of Earth and Space Sciences, University of Washington, Seattle, Washington, USA.
[3]Space Sciences Laboratory, University of California, Berkeley, California, USA.

0148-0227/03/2002JA009725$09.00

al., 2000] that emphasizes the near antiparallel alignment between a merging IMF and geomagnetic field. Another model, that seems to be more important at the dayside subsolar magnetopause [e.g., *Gosling et al.*, 1990], is the so-called component merging model that predicts reconnection when the shear between any single components of the magnetic field vectors is sufficiently large [e.g., *Gonzalez and Mozer*, 1974].

[5] Past studies of lobe reconnection at the high-latitude magnetopause have been focused mainly on northward IMF conditions and locations tailward of the cusp along the noon-midnight meridian, following the work of *Dungey* [1963]. Two recent reports, by *Onsager et al.* [2001] using Polar spacecraft data and by *Avanov et al.* [2001] using Interball Tail data, provide evidence of lobe reconnection for a northward IMF event on the same date, 29 May 1996. The former study used electron and ion phase space density signatures as indicators for reconnection and concluded that Polar was observing a prolonged ~6 hour period of reconnection at the high-latitude dayside magnetopause poleward of the cusp. It was also reported, somewhat surprisingly, that the magnetosheath field seemed to merge with either lobe or plasma sheet magnetic fields. The Avanov et al. study reported quasi-steady reconnection for ~10–12 min on an outbound magnetopause crossing from (X_{GSM}, Z_{GSM}) = (−1, 5) R_E to (X_{GSM}, Z_{GSM}) = (4, 9) R_E tailward of the cusp by Interball Tail using magnetic field data and ion density, temperature, and flow velocity as indicators of merging. An increased magnetic field and decreased ion density in the magnetosheath adjacent to the magnetopause made Avanov et al. suggest the formation of a plasma depletion layer [*Fuselier et al.*, 2000] as a cause of the reconnection site stability and the observed sub-Alfvénic sunward plasma flow.

[6] Recently, a few observations of B_y-dominated IMF reconnection has been presented as well. Using magnetic field data and proton density, temperature, and bulk speed data, *Marcucci et al.* [2000] reported an indirect observation of a several hours long reconnection event detected by the Equator-S spacecraft for a dawn magnetopause skimming orbit near the equatorial plane. Southward directed accelerated plasma flows, indicating a reconnection site at the dawn flank of the Northern Hemisphere, was reported for a predominantly dawnward directed IMF with a southward B_z component. *Popescu et al.* [2001] presented Interball Tail data of a reconnection event, also during mainly dawnward IMF, at the high-latitude dawnside magnetopause flank with a "sunward flowing plasma layer" adjacent to the plasma mantle in the midtail ($-9\ R_E < X_{GSM} < -15\ R_E$ and $Y_{GSM} \sim -10\ R_E$) that lasted for several hours. They concluded a source 15 R_E downtail or more for the observed magnetosheath ions and heated electrons.

[7] In a global MHD simulation study, using a strictly positive IMF B_y, *White et al.* [1998] discovered a region of low magnetic field, termed the magnetospheric sash, stretching tailward along the Northern dusk and the Southern dawn magnetopause flanks. An opposite geometry is expected for a negative IMF B_y. There is some evidence from recent in situ observations that the sash does exist and that it may be a site for reconnection of open field lines previously opened by dayside merging [*Maynard et al.*, 2001].

[8] A cross-polar auroral band of emissions in ultraviolet spectra, connecting the dayside and nightside part of the auroral oval, was first reported by *Frank et al.* [1982]. This auroral feature has been termed "transpolar aurora" or "theta aurora" in subsequent literature and is observed in a region of sunward convection [e.g., *Frank et al.*, 1986]. *Cumnock et al.* [1997] reported five events of transpolar aurora in the Northern Hemisphere during northward IMF that formed from expanded diffuse-like emission regions on the duskside (dawnside) for positive (negative) IMF B_y, as was suggested by *Hones et al.* [1989]. Following a shift in the sign of B_y, the transpolar aurora subsequently commenced drifting in the new direction of IMF B_y. *Makita et al.* [1991] reported the same IMF B_y-dependence of particle precipitation in the region between the transpolar aurora and the auroral oval which supports the proposed IMF B_y-dependent tail and plasma sheet rotation model about the Sun-Earth line [e.g., *Siscoe and Sanchez*, 1987; *Cowley et al.*, 1991] for transpolar auroral formation [e.g., *Meng*, 1981; *Jankowska et al.*, 1990; *Kullen*, 2000]. A rotation of the magnetotail in the YZ_{GSM} plane would bring the plasma sheet, and hence the boundary plasma sheet, up to higher latitudes and may explain the observations of precipitating plasma sheet-like particles in transpolar aurora [e.g., *Peterson and Shelley*, 1984], in the sunward convection region of lobe cells [e.g., *Eriksson et al.*, 2002], as well as the apparent plasma sheet origin, rather than lobe like, of plasma participating in high-latitude reconnection [e.g., *Huang et al.*, 1987; *Onsager et al.*, 2001]. Most observations of the generation of smaller-scale Sun-aligned arcs [e.g., *Valladares et al.*, 1994] or transpolar aurora note their close connection with the IMF [e.g., *Zhu et al.*, 1997], such as *Chang et al.* [1998], who suggest a model based on the antiparallel merging model that emphasizes the dependence on the B_y component of the IMF.

[9] In this paper, we present a composite study of low-altitude signatures of plasma convection from the FAST satellite [*Carlson et al.*, 1998] and simultaneous Polar UVI data [*Torr et al.*, 1995] that suggests a close connection between the two phenomena of lobe convection and polar cap precipitation, such as transpolar auroral features. The FAST satellite was launched on 21 August 1996 into an 83° inclination elliptical orbit of 350 km by 4175 km altitude with an orbital period of about 2 hours and 10 min. All Polar UV images utilized in this study applied the Lyman-Birge-Hopfield (LBH-long) filter centered at ~1700 Å for the molecular nitrogen lines.

2. Observations

[10] In a previous study [*Eriksson et al.*, 2002], we examined the local time dependence of the low-altitude electric and magnetic field signatures of lobe cell convection in the Northern Hemisphere using FAST observations and found a strong correlation with the IMF B_y component and the ratio $|B_y/B_z|$ being larger than one. A dawnside signature was observed for negative B_y, while a duskside signature was found for positive B_y. Moreover, we found that the origin of particle precipitation coinciding with the sunward convection part of the lobe cell could sometimes be interpreted as being magnetosheath-like and sometimes as plasma sheet-like [see e.g., *Newell et al.*, 1991, and references therein].

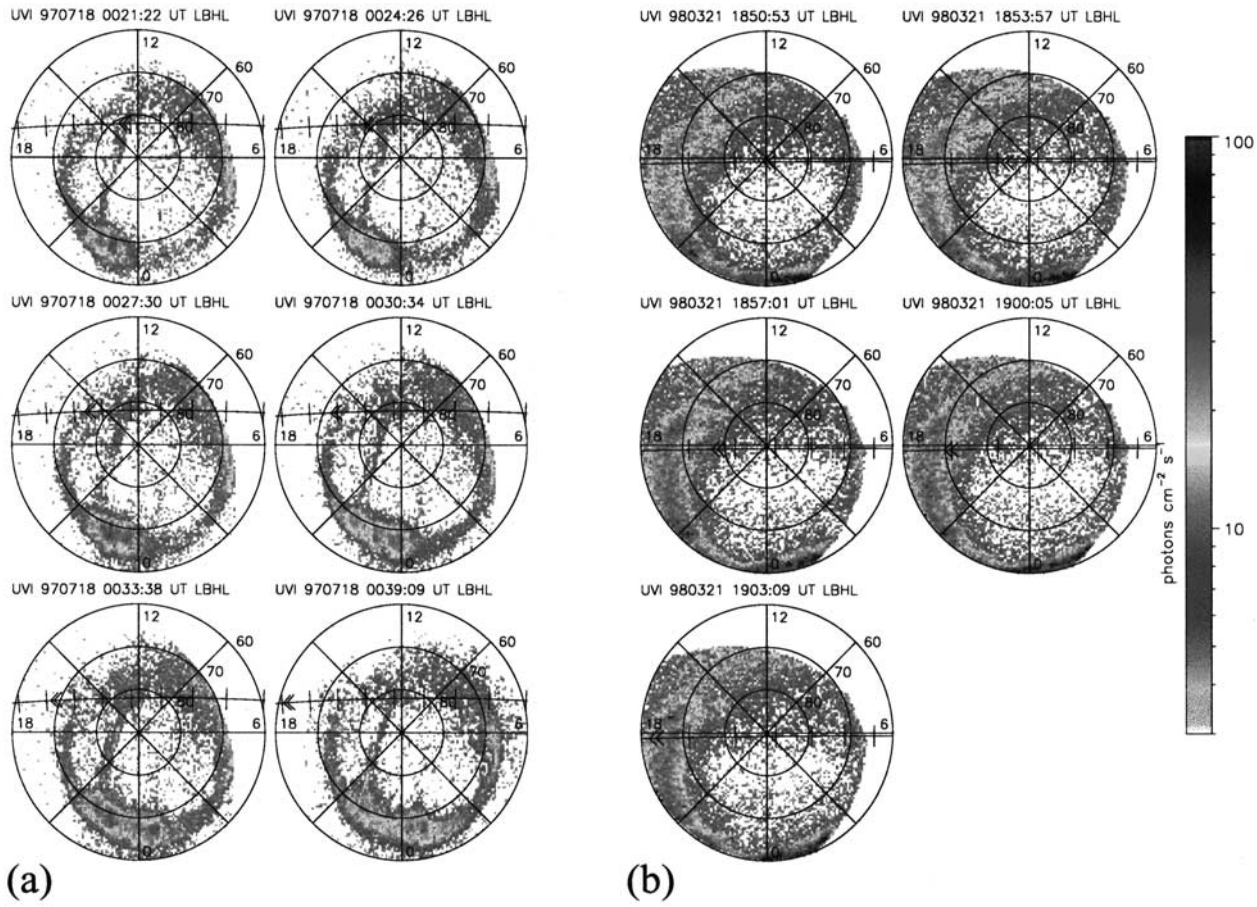

Figure 1. Polar UV images at the times of FAST orbits (a) 3575 and (b) 6246. FAST is moving from dawn to dusk as shown by the satellite track and the triangular marker that indicates the integration time interval for each Polar UV image. See color version of this figure at back of this issue.

[11] In the following section, we present detailed Polar UVI and FAST data for two duskside and two dawnside lobe cell convection events, respectively, and compare the signatures of polar cap particle precipitation as observed by FAST and Polar UVI with IMF data from the Wind upstream solar wind monitor. The footpoint of the geomagnetic field along a smaller section of the FAST orbit for these events are further mapped into the magnetotail lobes using the T01 model [*Tsyganenko*, 2002] of the geomagnetic field. The case study is followed by a statistical survey of 55 FAST events and 34 concurrent Polar UVI cases in the Northern Hemisphere. The set of 55 events, which includes the four detailed cases, were selected based on their magnetic field signature in FAST data indicating the presence of four large-scale field-aligned currents on either the dawnside or the duskside of the noon-midnight meridian plane [*Ohtani et al.*, 1995; *Eriksson et al.*, 2002]. The along-track electric field was then utilized to confirm the existence of convection reversal boundaries in the region of these field-aligned currents.

2.1. Case Study

[12] Figure 1 depicts Polar UVI data and the projection of the FAST orbit for two examples that displays a lobe cell signature in the electric and magnetic field data on the duskside for positive IMF B_y. FAST crosses the polar cap from dawn to dusk as seen by the pair of two arrows that marks the distance covered by the FAST footpoint during the UV integration interval, while an evenly distributed vertical bar marks each 5-min time step. A distinct transpolar arc is present on the duskside and FAST (orbit 3575) is in direct conjunction with this feature at 00:21:22 UT (Figure 1a). We also note a substorm-like auroral oval intensification in the premidnight sector where the transpolar arc attaches to the oval. The transpolar arc developed about two hours earlier from the premidnight 2000–2400 MLT auroral oval during a substorm and began bending toward noon during the latter part of the previous FAST orbit 3574 (not shown). It seems furthermore that a westward section of the particle precipitation region causing the oval UV enhancement convects sunward onto the transpolar arc at 00:39:09 UT. Features such as this premidnight intensification spot are often observed together with transpolar aurora and are sometimes also detected near 1500 MLT [e.g., *Murphree et al.*, 1987; *Liou et al.*, 1999]. The UV image for FAST orbit 6246 (Figure 1b) does not show a transpolar arc, however. Instead, we observe diffuse-like UV emissions poleward of the duskside auroral oval reminiscent of a duskside section of the "horse-collar aurora" [*Hones et al.*, 1989] and much of the visible oval indicates

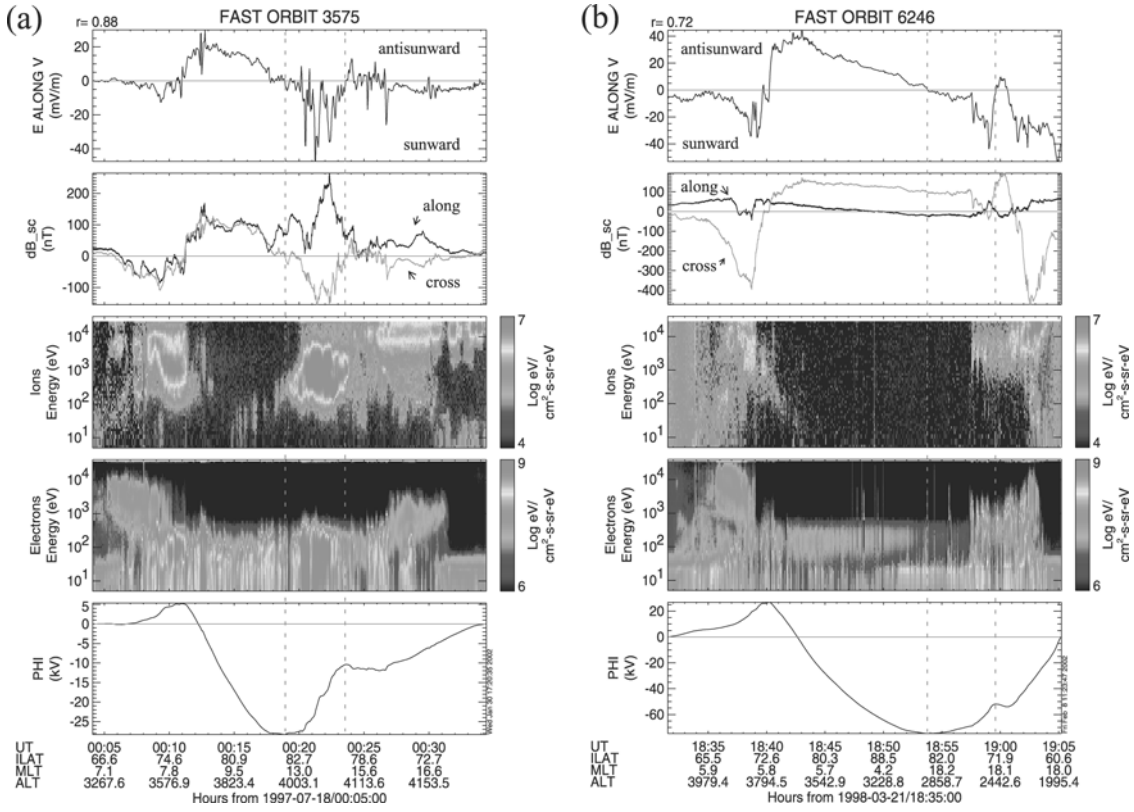

Figure 2. Two examples of lobe cell convection as observed by FAST on the duskside for positive IMF B_y, (a) FAST orbit 3575 and (b) FAST orbit 6246. The top two panels show the along-track electric field and the magnetic field (green is perpendicular, and black is along the direction of motion). The precipitating ion and electron energy flux versus energy and time are followed by the integrated electric field assuming a return to zero potential. Vertical dashed lines indicate the equatorward interval of sunward lobe convection. See color version of this figure at back of this issue.

an ongoing substorm. Horse-collar aurora is the name given to UV images that displays the combined features of an auroral oval and a region of diffuse auroral emissions immediately poleward of the oval on both the morningside and eveningside. The diffuse regions are often bounded by a distinct Sun-aligned bar of more intense emissions on their polar cap edges, either on the morningside or the eveningside, or both.

[13] The composite set of FAST observations for these two events are shown in Figure 2. The five panels correspond to the along-track electric field, the cross-track (green) and along-track (black) perturbation magnetic field, the energy-time spectra for precipitating ions and electrons within 20° of the local magnetic field direction, and the integrated electric field. A constant electric field on the order of ~1–2 mV/m, corresponding to the potential offset at the end of the polar cap pass, was added to the measured electric field in a prior analysis. The contribution of the corotation electric field to the total measured field was further subtracted to focus our attention on the convection electric field. The perturbation magnetic field dB_{sc} in a spacecraft coordinate frame of reference is obtained as the difference between the measured magnetic field and the International Geomagnetic Reference Field. The electric fields between the dashed vertical lines are negative (sunward $\vec{E} \times \vec{B}$ convection) on the poleward side of a region of weakly positive electric field (antisunward $\vec{E} \times \vec{B}$ convection) that suggest a lobe cell adjacent to a "viscous cell" [e.g., *Burch et al.*, 1985]. The perturbation magnetic field signatures perpendicular to the satellite track (green line in second panel from the top) are well-correlated with the along-track electric fields as shown by the high correlation coefficients (upper left corner of each plot) and indicates the presence of four large-scale field-aligned currents [*Ohtani et al.*, 1995; *Eriksson et al.*, 2002] near the convection reversal boundaries, which are defined here by large-scale zero electric field crossings. The energy of precipitating ions and electrons in the sunward convection region of the lobe cell (between the dashed lines), however, show two rather different features. In one case (Figure 2a, orbit 3575) the ion energy-time spectra is magnetosheath-like between ~00:20 and 00:23 UT, as confirmed by the ion number flux versus energy distribution (not shown), while the other case (Figure 2b, orbit 6246) indicates boundary plasma sheet-like energy fluxes from ~18:57 to 18:59 UT [*Newell et al.*, 1991] that coincides with enhanced sunward convection at the equatorward end of the interval. The precipitating magnetosheath-like energy fluxes observed during orbit 3575 is seen to coincide with the transpolar arc on sunward $\vec{E} \times \vec{B}$ convection (Figure 1a, 00:21:22 UT). Diffuse auroral emissions present in the UVI during orbit 6246 from ~18:57 until 18:59 UT (Figure 1b) lines up with FAST

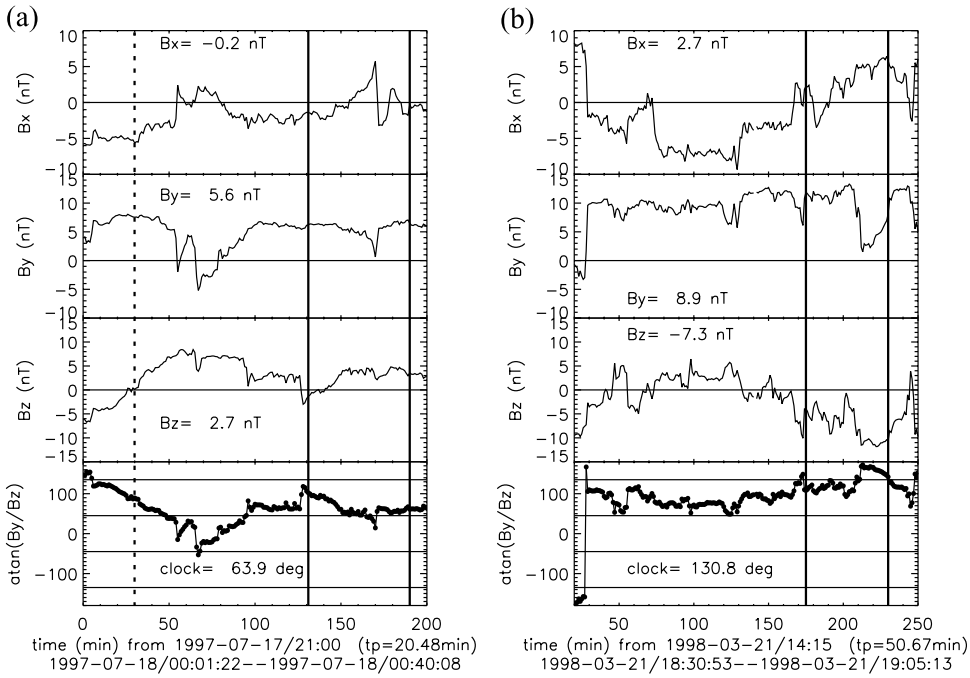

Figure 3. The time-shifted IMF (see text for details) in GSM coordinates corresponding to FAST passes (a) 3575 and (b) 6246 is highlighted between the two vertical lines as well as the clock angle $\theta = \arctan(B_y/B_z)$. Four horizontal lines in the θ panel mark the levels of $\theta = -135°$, $\theta = -45°$, $\theta = 45°$, and $\theta = 135°$. Average values taken between the vertical lines of the three components of the IMF and of θ are shown in each panel. The estimated propagation time and the local time interval in UT for the FAST passes are found below the two plots.

observations of enhanced sunward $\vec{E} \times \vec{B}$ convection and plasma sheet-like precipitation toward the end of the interval of sunward convection. A drop out in the polar rain fluxes is further noted on the duskside between 18:53 and ~18:57 UT, centered around the lobe cell convection reversal boundary. A similar polar rain drop out was documented by *Sandholt et al.* [2003] on 3 December 1997 in the region of the center of the lobe cell. Evidence of a dawn-dusk asymmetry in polar rain intensity was given by *Meng et al.* [1977]. A higher intensity was typically observed near dawn (dusk) for positive (negative) IMF B_y in the Northern Hemisphere, as is observed here for positive IMF B_y.

[14] The time-shifted 1 min resolution IMF data in GSM coordinates from the Wind monitor corresponding to both these events are displayed in Figure 3. The top three panels show the three components of the IMF and the bottom panel displays the IMF clock angle $\theta = \arctan(B_y/B_z)$ where horizontal lines are drawn for $\theta = -135°$, $-45°$, $45°$, $135°$. A clock angle of 90° (−90°) corresponds to IMF $B_z = 0$ and a positive (negative) B_y. The average Wind GSE location on 1997-07-18 was (85, −15, −8) R_E and at (231, −24, −14) R_E on 1998-03-21. The estimated propagation times are 20.48 min (Figure 3a) and 50.67 min (Figure 3b), respectively. Following *Weimer* [2001], the total time shift of the data accounts for the propagation of the solar wind from Wind to an average upstream magnetopause at 10 R_E, a presumed 10 min communication time delay from the magnetopause to the ionosphere, and a global 20 min reconfiguration time delay of the ionosphere applied only to the first encounter with the low-altitude convection electric field at the beginning of the polar cap crossing. The time interval between the two vertical lines in Figure 3 thus correspond to FAST being poleward of 60° invariant latitude (ILat). The averages of the IMF components during these intervals are shown in each panel and we observe that both events occurred for a predominantly positive IMF B_y. This is also illustrated by an average clock angle of $\theta = 63.9°$ and $\theta = 130.8°$, respectively. Note that the clock angle is expected to be in the range from $|\theta| = 45°$ to $|\theta| = 135°$ as the IMF B_z component rotates through zero while IMF B_y remains the dominant component. During these two intervals, IMF B_z is either northward or southward following a change in direction, while IMF B_y stays positive. These events may therefore not be classified as typical "theta aurora" cases, occurring for generally steady and dominant IMF $B_z > 0$ and moving across the polar cap in the direction of IMF B_y upon a change in its direction [*Cumnock et al.*, 2002]. It was pointed out by *Newell and Meng* [1995] that a switch in the direction of IMF B_z from north to south after a prolonged period of northward IMF seemed to produce theta aurora. We observed a similar shift in IMF B_z just prior to the estimated IMF time interval of FAST orbit 6246, but with resulting diffuse UV auroral emissions (Figures 1b and 3b). The temporal evolution of the IMF corresponding to the distinct transpolar aurora indicates a narrow interval of southward IMF B_z at the beginning of FAST orbit 3575 (Figures 1a and 3a). However, the transpolar arc developed much earlier during FAST orbit 3574 at the time of a clear transition from southward to northward IMF as indicated by the dashed vertical line in Figure 3a. This is the opposite IMF B_z transition from what you would expect from the

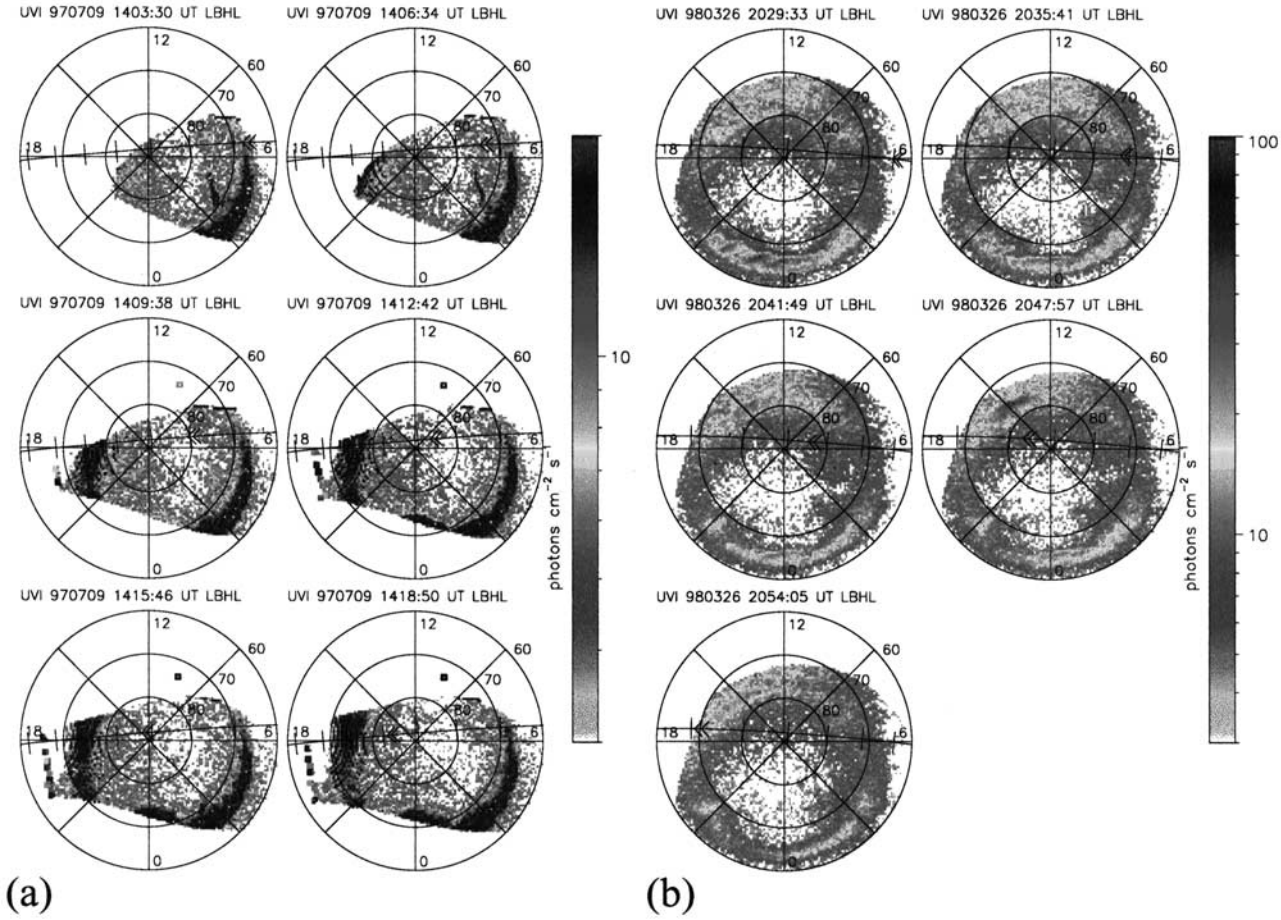

Figure 4. Polar UVI for FAST orbits (a) 3484 and (b) 6301. Same format as Figure 1. A different photon flux scale is used for the UV image on the left to enhance the transpolar arc feature on the dawnside of the polar cap. See color version of this figure at back of this issue.

results of *Newell and Meng* [1995]. It may be that the temporary dawnward shift in IMF B_y in between these two FAST orbits separated the transpolar arc from the oval and that it began drifting toward the dawnside until the IMF B_y returned to a duskward direction [e.g., *Cumnock et al.*, 1997].

[15] Contrasting the two previous events for positive IMF B_y, we now show two events occurring on the dawnside for negative IMF B_y. The Polar UV image obtained during FAST orbit 3484 (Figure 4a) indicates the presence of a structured Sun-aligned feature emanating on the nightside of the dawnside oval during substorm conditions. FAST is passing in the sunward direction of this feature at about 14:09:38 UT or somewhat earlier. Note that this UVI signature fades away after this time. The UV image for orbit 6301 (Figure 4b, note the different photon flux scales) on the other hand suggests a broad region of diffuse-like asymmetric polar cap emissions, as was the case for the duskside diffuse particle precipitation event (Figure 1b, orbit 6246), but now located in the dawnside polar cap. Note also the presence of an auroral intensification region in the UV image at 20:47:57 UT between ~1300 and 1600 MLT.

[16] Figure 5 depicts the same set of low-altitude FAST observations as in Figure 2. The time interval between the dashed vertical lines at 14:08 UT and ~14:10 UT for orbit 3484 (Figure 5a) corresponds to the low-latitude sunward convection part of a lobe cell located poleward of a "viscous cell" following *Burch et al.* [1985] and is observed to coincide with boundary plasma sheet-like precipitation poleward of the higher energy electron precipitation of the central plasma sheet. This precipitation is detected sunward of the protruding Sun-aligned UV feature, suggesting that this structure may in fact extend sunward as a transpolar arc, but below the detection threshold of the UVI instrument. The dawnside electric field for orbit 6301 (Figure 5b) indicates a lobe cell signature as well with sunward lower latitude convection observed between 20:36 UT and ~20:42 UT (dashed lines), which is almost a mirror image of the duskside electric field signature of orbit 6246 (Figure 2b). The electron precipitation is once again boundary plasma sheet-like until 20:38 UT. Precipitation poleward of this location and centered at the convection reversal boundary of the lobe cell at about 20:42 UT suggests a large-scale ~1800 km wide inverted V-like event similar to what we observed for two passes that crossed through the "1500 MLT spot" (FAST orbits 3553 and 3585, not shown). The entire interval of sunward convection as observed by FAST between the dashed lines coincides with the poleward part of the broad diffuse-like UV emission region. The wide

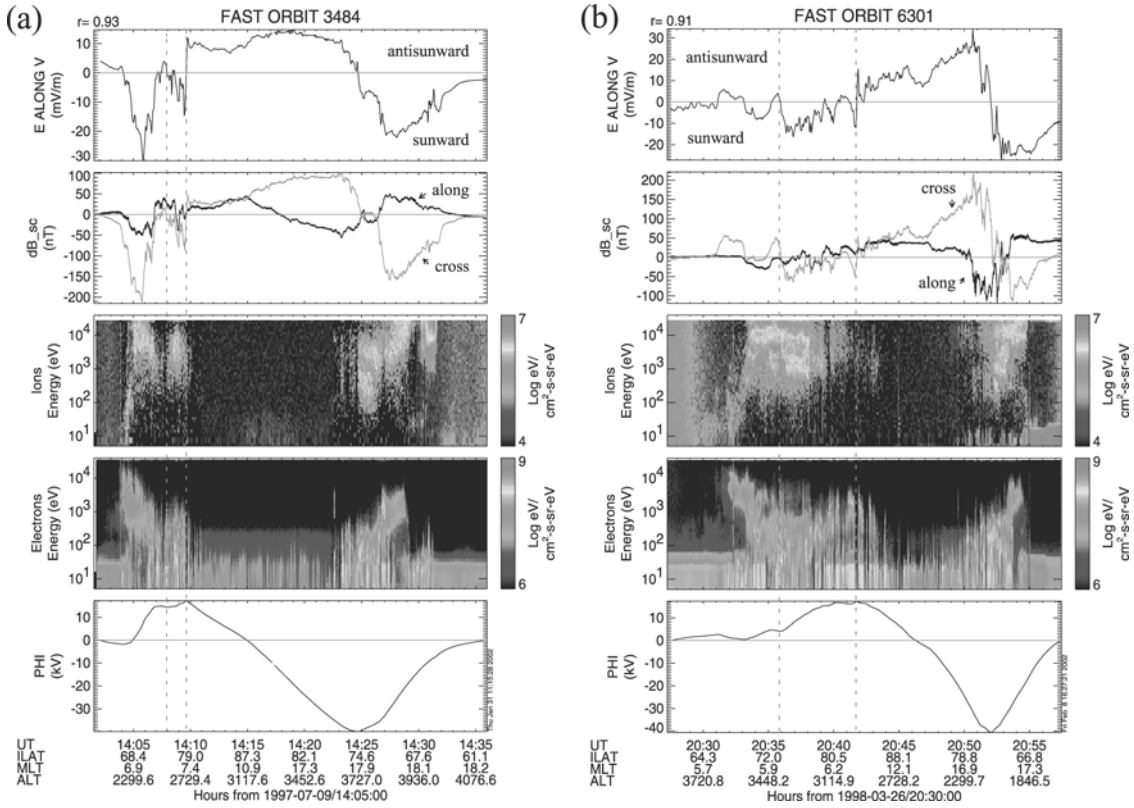

Figure 5. Two examples of lobe cell convection as observed by FAST on the dawnside for negative IMF B_y, FAST orbits (a) 3484 and (b) 6301. Same format as Figure 2. See color version of this figure at back of this issue.

dawnside inverted-V signature is not clearly resolved in the UVI, however, unlike the "1500 MLT spot." The electron precipitation recorded during orbit 6301 shows, moreover, a polar rain drop out, but now toward the dawnside with higher intensities near dusk between 20:48 UT and 20:50 UT.

[17] The IMF data corresponding to these two events are shown in Figure 6, and despite the data gap in Wind data for orbit 3484 (Figure 6a), there are once again clear indications for the importance of the IMF B_y and $-135° < \theta < -45°$ for lobe cell convection and the coinciding particle precipitation. The Wind data corresponding to orbit 3484 were shifted by a propagation time delay of 16.62 min as well as the assumed 10 min communication delay and the 20 min global reconfiguration time delay, applied only to the earlier boundary, from its GSE location at (63, −41, −5) R_E. The corresponding propagation time delay for FAST orbit 6301 was estimated at 42.53 min from an average Wind location at (230, −23, −9) R_E (Figure 6b). There is no clear IMF B_z shift prior to FAST orbit 6301. However, it may be that the southward turning of the IMF B_z ~70 min prior to the IMF corresponding to FAST orbit 3484 (vertical dashed line) together with the temporary duskward shift of IMF B_y following the B_z transition initiated the Sun-aligned protrusion of UV emissions in the Polar UVI data.

[18] Figure 7 illustrates the convection $\vec{E} \times \vec{B}$ drift velocity using the measured along-track electric field and the IGRF model magnetic field for the four cases analyzed above. The global maximum and minimum in the cross-polar potentials are marked by solid shaded dots and the approximate locations of the lobe cells are indicated by grey ellipsoids following the schematic *Burch et al.* [1985] convection model. In comparing these drift patterns with the Polar UVI images, we observe that the lower latitude sunward convection sections of the lobe cells coincide favorably with the transpolar arc (Figures 1a and 7a), the imagined extension of the emanating auroral feature from the dawnside oval (Figures 4a and 7c), and the poleward part of the diffuse-like UV auroral emissions on the duskside (Figures 1b and 7b) and the dawnside (Figures 4b and 7d), respectively. This is further illustrated in Figure 8 showing FAST orbit 3553 crossing the polar cap from dawn to dusk, where the Polar UVI indicates an extended region of diffuse-like emissions poleward of the duskside auroral oval. This UV image further illustrates an example of a transpolar auroral feature developing on the boundary between the polar cap (defined here as the low-emission region) and the diffuse emission region, as was proposed by *Hones et al.* [1989]. The estimated average IMF (B_x, B_y, B_z) during this event was (−2.6, 9.1, −0.7) nT with an average clock angle of $\theta = 94.2°$. Furthermore, the clock angle had stayed between 45° and 135° during ~75 min prior to this time interval. Note that the diffuse emission region coincides with sunward $\vec{E} \times \vec{B}$ convection. The maximum $\vec{E} \times \vec{B}$ velocity vector shown is 3.6 km/s. Moreover, the duskside minimum in the cross-polar cap potential is located above 80° ILat and poleward of the diffuse emission region as would be expected from a duskside lobe

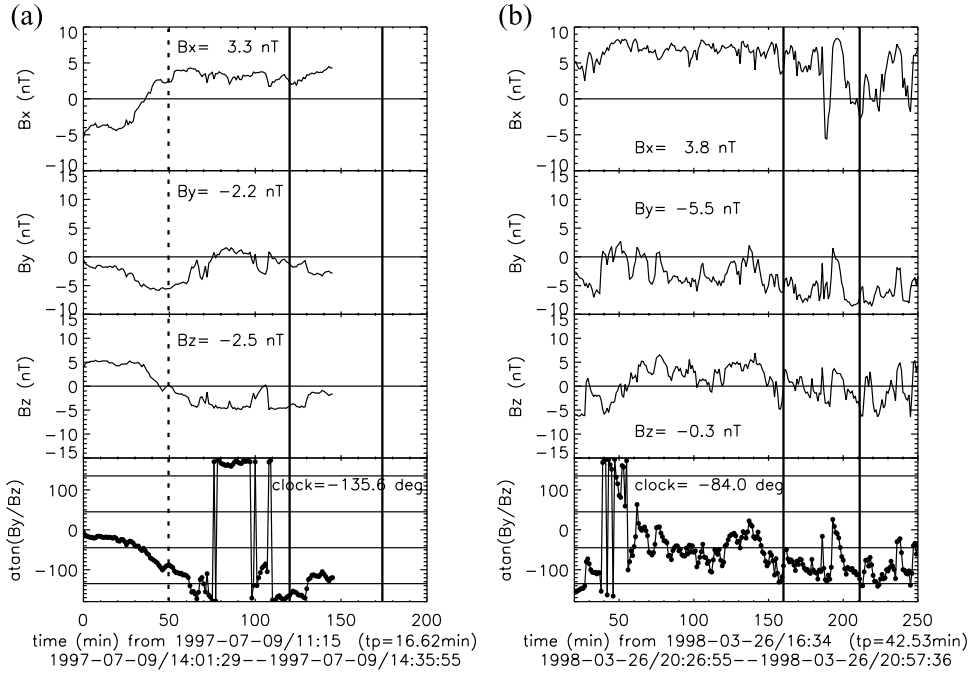

Figure 6. Time-shifted IMF for two FAST cases of lobe cell convection signatures on the dawnside, (a) orbit 3484 and (b) orbit 6301. Same format as Figure 3. Although there is a data gap in the Wind data during the second half of the interval for orbit 3484, B_y is negative during the first ∼25 min.

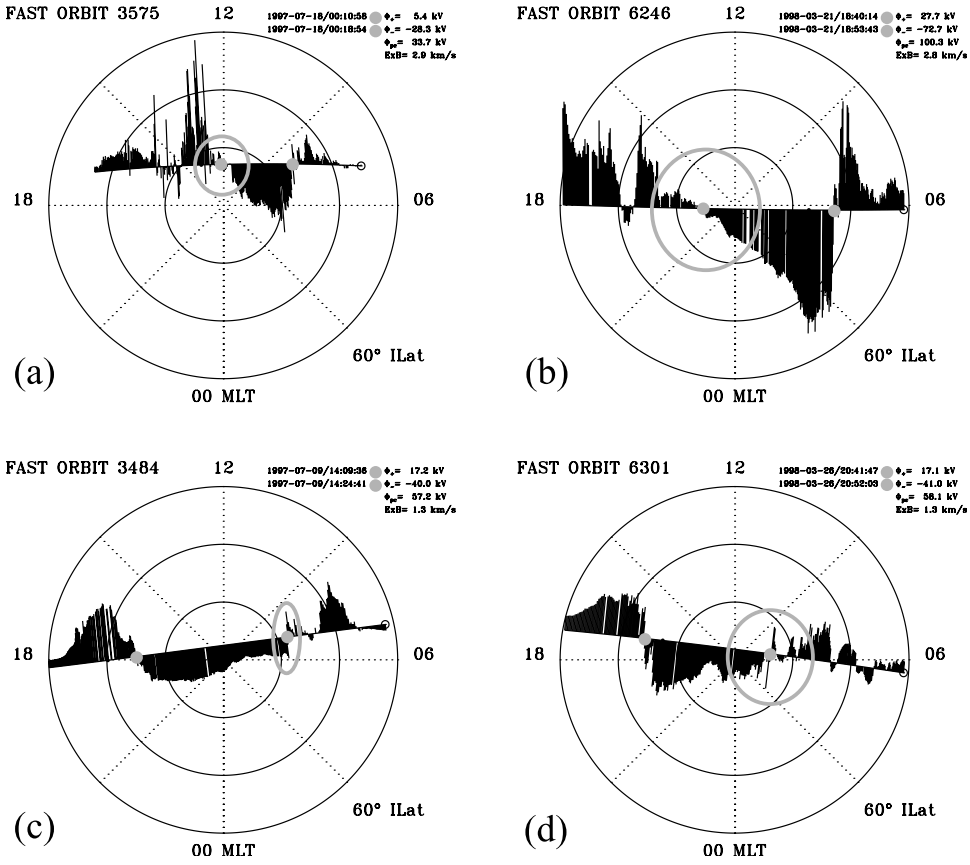

Figure 7. Convection $\vec{E} \times \vec{B}$ drift velocity for orbits (a) 3575, (b) 6246, (c) 3484, and (d) 6301. Maximum drift velocities shown are 2.9, 2.8, 1.3, and 1.3 km/s, respectively. Shaded dots mark the locations of the calculated global cross-polar potential maxima, and shaded ellipsoids indicate the approximate sites of lobe cells.

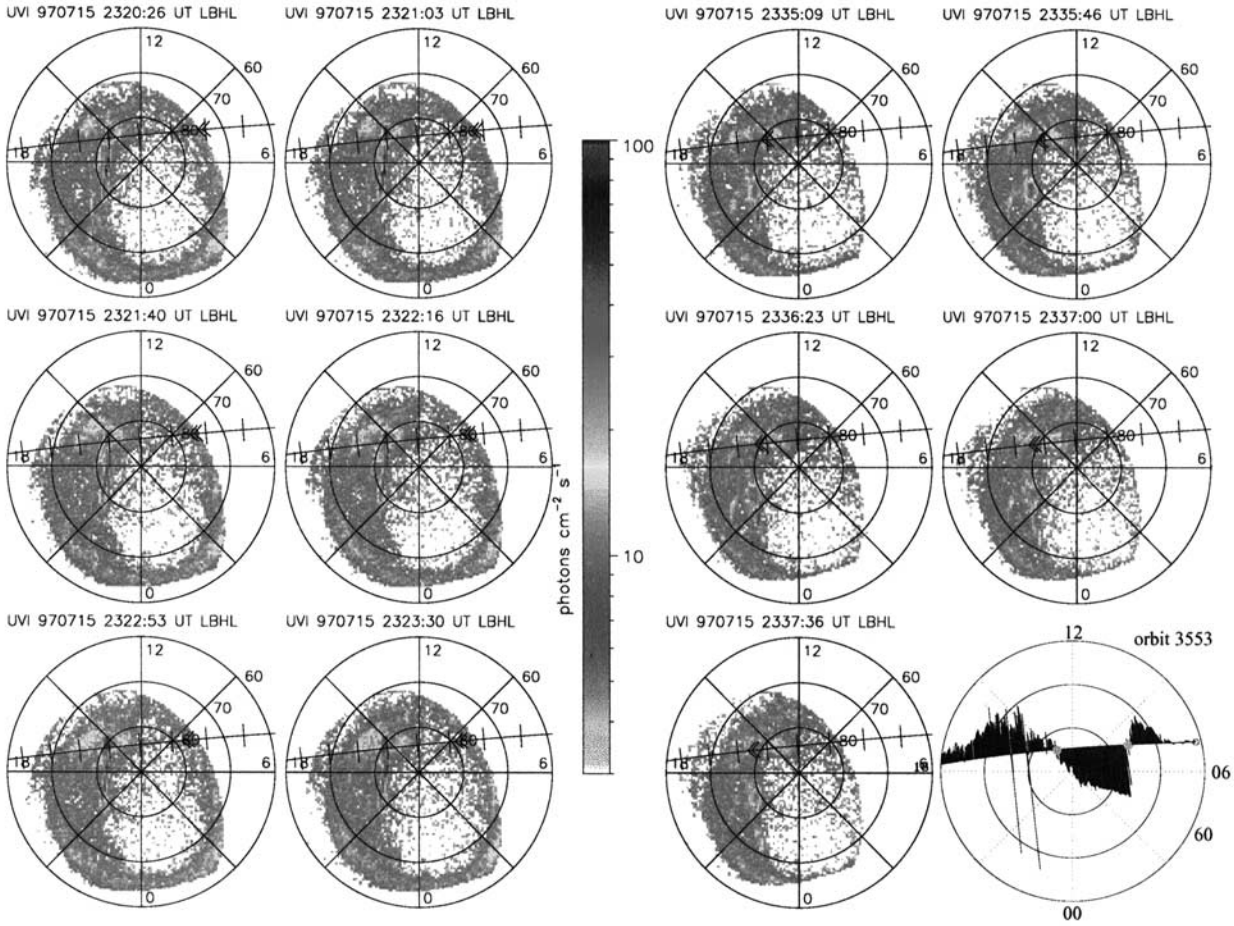

Figure 8. Polar UVI for FAST orbit 3553 from 1997-07-15 (read as 15 July 1997) 23:20:26 UT (top left) to 23:37:36 UT (bottom right). The corresponding $\vec{E} \times \vec{B}$ convection velocity is shown after the complete time sequence. Maximum shown drift velocity is 3.6 km/s. Note the transpolar-like auroral arc signature that develops on the border between the polar cap and the diffuse-appearing emissions on its equatorward side. See color version of this figure at back of this issue.

cell. This minimum coincides rather well with the location of a 1500 MLT spot in the UVI data when FAST measured an inverted V-like electron event (not shown), such as the one illustrated for orbit 6301 (see Figure 5b). It seems also that the duskside viscous cell is too weak in comparison with the lobe and dayside merging cells to appear, as it did, however, in the previous cases (see Figure 7) with an antisunward viscous convection region just equatorward of the sunward lobe cell convection. *Hones et al.* [1989] further reported that the region of diffuse emissions sometimes faded, leaving only the brighter transpolar arc. There are some differences between their observations and the present study, though. First, they reported a symmetric system of two regions occurring simultaneously on the dawnside and the duskside. Second, their observations were performed during quiet geomagnetic conditions for $AE < 50$ nT and probably correspond to dominant northward IMF B_z conditions, unlike the IMF B_y dominant situations reported here.

[19] The question is to what regions of the magnetosphere that the lower-latitude sunward lobe cell convection most probably maps to. We used the T01 model [*Tsyganenko*, 2002] along with the observed average solar wind conditions from Wind when FAST was above 60° ILat to trace the magnetic field lines along the orbital track during the time periods when FAST passed these sunward lobe convection regions observed between the dashed lines in Figures 2 and 5. Figure 9 illustrates the magnetic field lines corresponding to the four events described in detail previously and presented in the XZ_{GSM}, YZ_{GSM}, and XY_{GSM} planes. The times explicitly shown in Figure 9 correspond to the first and the last traced field lines in the interval of ionospheric sunward lobe convection. It is seen that the field lines for the two IMF $B_y > 0$ events (Figures 9a and 9b) map toward the duskside Northern Hemisphere tail lobe flanks, while the two IMF $B_y < 0$ events (Figures 9c and 9d) map to the dawnside tail lobe flanks, respectively. Note that field lines that appear to map into the inner magnetosphere in the XZ_{GSM} plane actually map to the lower latitude magnetopause flanks as viewed in the YZ_{GSM} and XY_{GSM} planes. The tilted solid and dashed lines drawn in the YZ_{GSM} planes of the middle column indicate the range of expected clock

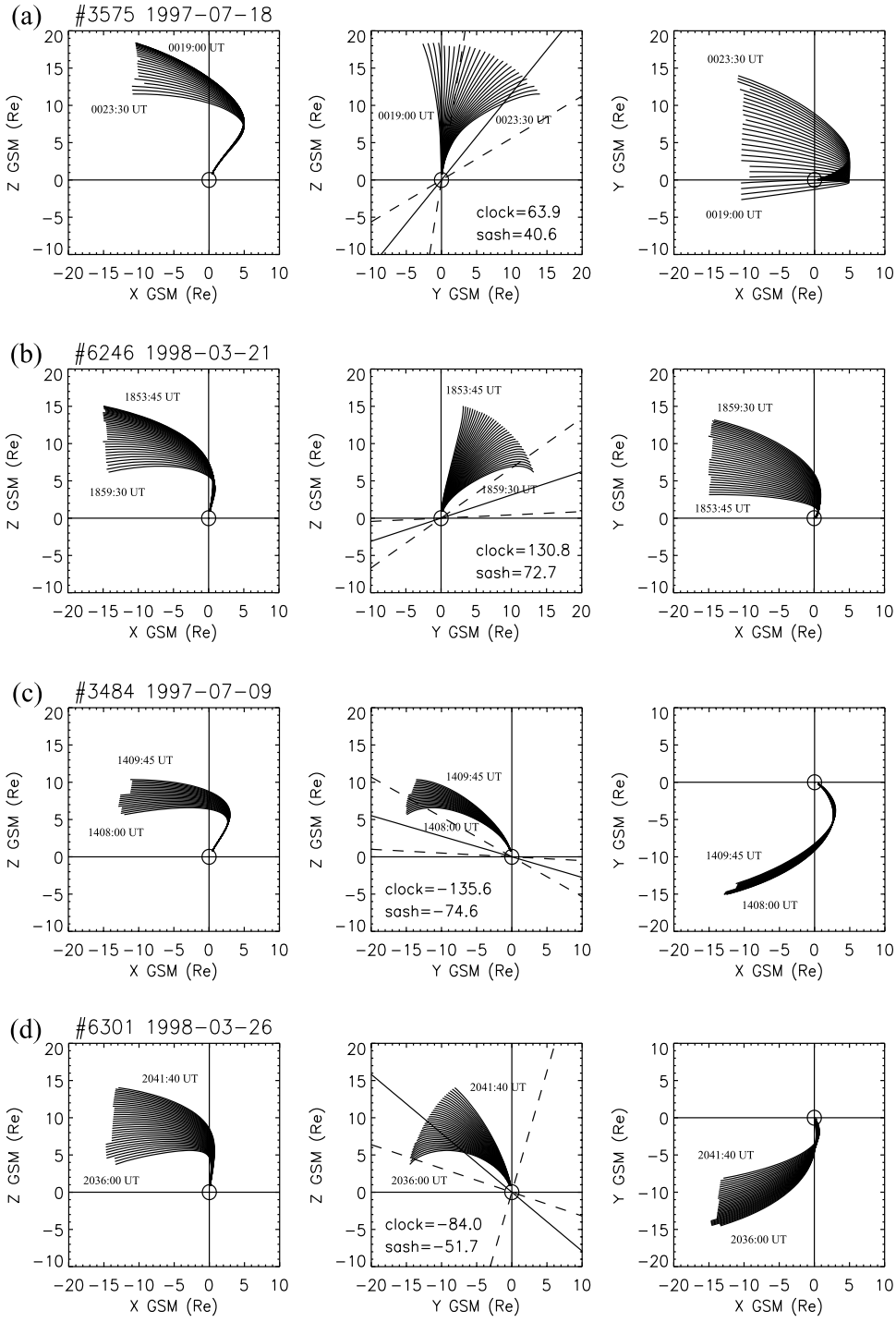

Figure 9. Mapping of sunward lobe cell convection regions into the GSM *XZ*, *YZ*, and *XY* planes using the *Tsyganenko* [2002] T01 model: (a) FAST orbit 3575 from 00:19:00 UT to 00:23:30 UT on 1997-07-18 (read as 18 July 1997) for mean IMF $\theta = 63.9°$, (b) FAST orbit 6246 from 18:53:45 UT to 18:59:30 UT on 1998-03-21 for $\theta = 130.8°$, (c) FAST orbit 3484 between 14:08:00 UT and 14:09:45 UT on 1997-07-09 for $\theta = -135.6°$, and (d) FAST orbit 6301 between 20:36:00 UT and 20:41:40 UT on 1998-03-26 for $\theta = -84.0°$. The tilted lines correspond to the expected clock angles of the magnetospheric sash for the minimum (dashed), mean (solid), and maximum (dashed) of the IMF clock angles (see text for more details).

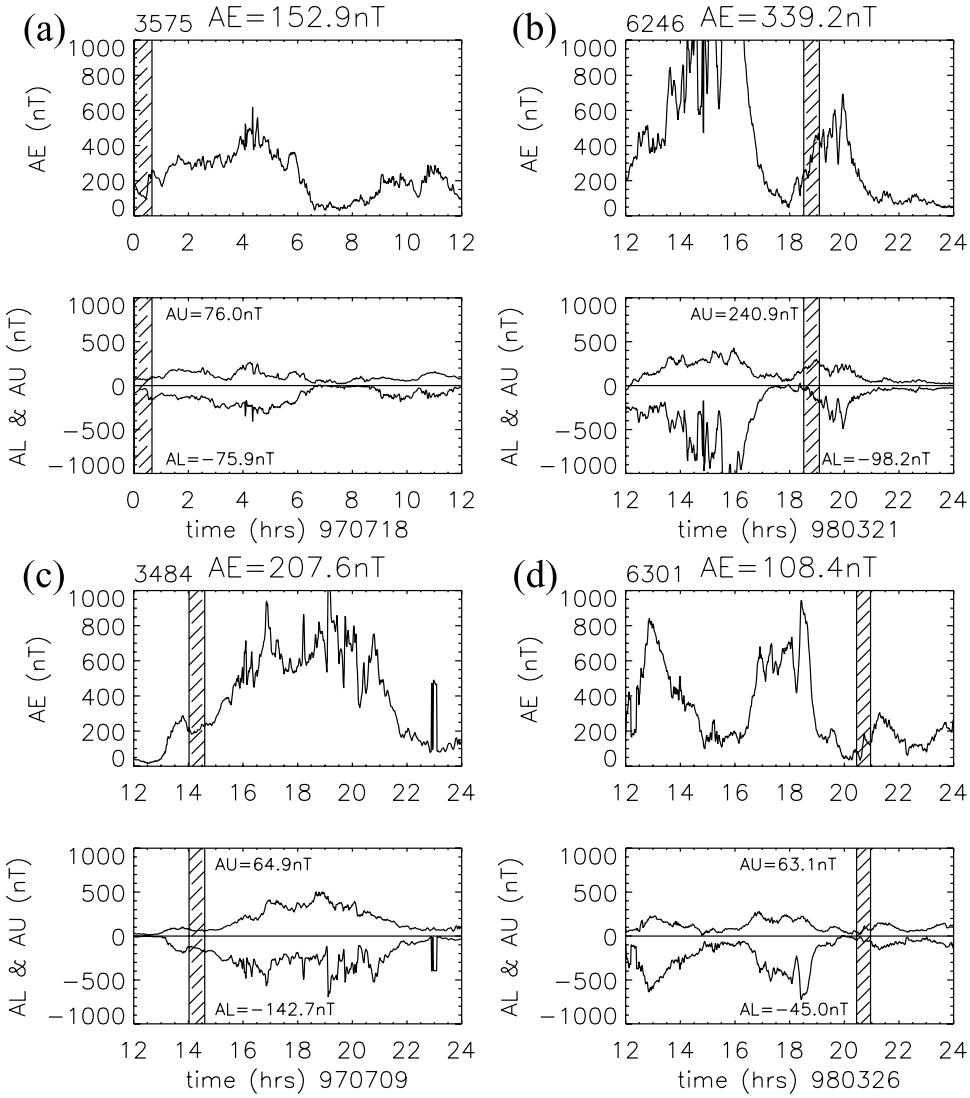

Figure 10. Provisional *AU*, *AL*, and *AE* indices versus time (hrs) for each corresponding event: (a) orbit 3575 on 1997-07-18, (b) orbit 6246 on 1998-03-21, (c) orbit 3484 on 1997-07-09, and (d) orbit 6301 on 1998-03-26. The average indices during each FAST pass (vertical bar) are shown on top of each plot.

angles of the magnetospheric sash at $X_{GSM} = 0$, using the minimum, mean, and maximum of the propagated Wind IMF clock angles when FAST is above 60° ILat (see Figures 3 and 6) as input to the expression

$$\tan(\theta_{mp}) = -\left(3 \pm \sqrt{9 + 8\tan^2(\theta)}\right)/2\tan(\theta) \qquad (1)$$

given by *Siscoe et al.* [2001a]. Here θ_{mp} is the clock angle of the magnetopause null points from a superposition of a uniform IMF with the Earth's dipole field in vacuum [*Crooker et al.*, 1990] and θ is the IMF clock angle. The minus sign applies for $0° \leq |\theta| \leq 90°$ and the plus sign applies for $90° \leq |\theta| \leq 180°$. It is assumed that the Earth's dipole is parallel to the Z_{GSE} axis and perpendicular to the solar wind flow. *Siscoe et al.* [2001a] showed that the resulting clock angles of the sash at $X_{GSM} = 0$ from their MHD code nearly matched θ_{mp}. Note that this angle increases toward 90° downtail from $X_{GSM} = 0$ and eventually merges with the tail neutral sheet [*White et al.*, 1998]. By comparing the location of the traced *Tsyganenko* [2002] T01 model field lines from the YZ_{GSM} perspective with the range of sash angles we observe that the field lines for two events (Figures 9a and 9d) map within a favorable sash region, while the other two events (Figures 9b and 9c) are less favorable. However, note that equation (1) does not take into account the effects of the dipole tilt angle. Moreover, the response time of the assumed dynamic sash region to the IMF clock angle is another unknown parameter.

[20] As noted above, it seems that there is some ongoing substorm-like activity in the Polar UV images coinciding with these events. Provisional *AE* and *AL* indices for 1997-07-18 and 1998-03-21, shown in Figures 10a and 10b, indicate that both duskside events occurred during substorm-like conditions (D. N. Baker, private communication), as suggested by the increased *AE* indices and the negative slope in the *AL* indices that may correspond to a

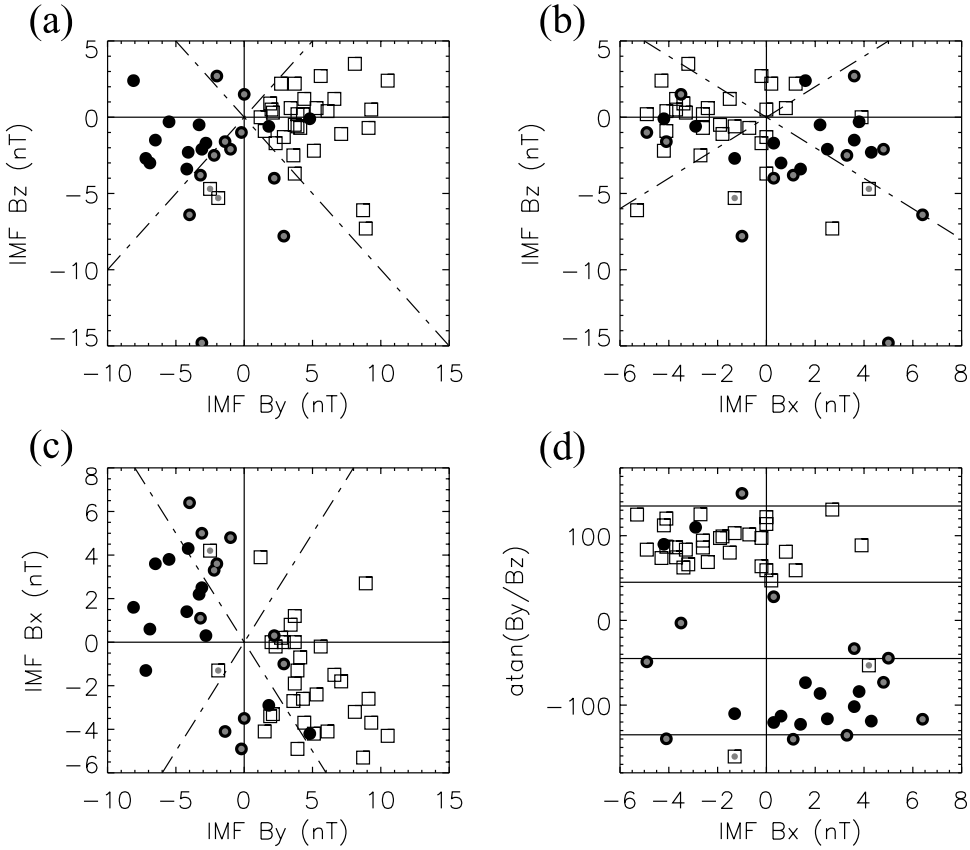

Figure 11. Average IMF distributions for 23 morningside events (dot) and 32 eveningside events (square): (a) B_z versus B_y, (b) B_z versus B_x, (c) B_x versus B_y, and (d) the average of the IMF clock angle $\theta = \arctan(B_y/B_z)$ versus B_x. Shaded dots represent events with $|B_y/B_z| < 1$ using the averaged B_y and B_z values (a).

possible expansion phase. The average *AE* indices for orbits 3575 and 6246 (taken between the vertical bars in Figures 10a–10b) are 153 nT and 339 nT, respectively. The average provisional *AE* indices for the dawnside events (Figures 10c and 10d) are 208 nT and 108 nT, respectively, indicating substorm-like activity for orbits 3484 and 6301 as well.

2.2. Statistical Survey

[21] The correspondingly averaged IMF for 55 FAST events that show an electric field and magnetic field signature in the Northern Hemisphere similar to those presented above are shown in Figure 11. These events were selected based on the magnetic field signature indicating the presence of four large-scale field-aligned currents on either the dawnside (black dots) or the duskside (squares) of the polar cap [*Ohtani et al.*, 1995; *Eriksson et al.*, 2002] during March, July, and November 1997, March 1998, and July 1998, when FAST was orbiting in the dawn-dusk meridian plane. A majority of events suggests a strong correlation with $|B_y| > |B_z|$ (Figure 11a). Of all 13 events with $|B_z| > |B_y|$ (a symbol with a shaded dot), 9 events occurred for $|B_x| > |B_y|$ (Figure 11c), suggesting the importance of both IMF B_x and B_y components for lobe cell convection and an antiparallel merging geometry. Figure 11d shows that six of these 13 cases having an average $|B_z| > |B_y|$ do have an average clock angle in the range $45° < |\theta| < 135°$ for the averaging Wind time intervals (see Figures 3 and 6). The average θ is thus within the B_y dominant interval for ~87% of all 55 examined cases. Figure 11a further shows that there are 19 morningside events and only two eveningside events when IMF $B_y < 0$. When $B_y > 0$ there are just four morningside events, but 30 eveningside ones. The FAST particle measurements in the sunward lobe convection regions suggest that the magnetospheric source of particle precipitation is most often plasma sheet-like (33 cases) with fewer cases indicating a magnetosheath-like source (16 cases). Six cases of all 55 events showed no clear evidence of particle precipitation.

[22] The results of a visual inspection of the distribution of polar rain intensity across the polar cap for all 55 events is found in Table 1, where "m" and "e" refer to morningside and eveningside lobe cell events, respectively. The

Table 1. Distribution of Polar Rain Intensity Over the Polar Cap[a]

m	e	description
6	1	duskside polar rain
1	18	dawnside polar rain
5	6	evenly distributed
8	1	no polar rain
3	6	unclear

[a]The first and second columns correspond to the 23 morningside (m) events and the 32 eveningside (e) events, respectively. "Duskside polar rain" refers to higher intensity polar rain near dusk.

dawn-dusk asymmetry of polar rain and its dependence on IMF B_y is clearly evident for the ~50% of cases showing a clear polar rain dispersion on either side of the polar cap region. Eleven cases showed an evenly distributed polar rain precipitation, while nine cases did not indicate any polar rain. Nine cases were unclear due either to structured higher-energy electron precipitation masking any polar rain signatures, or due to data gaps.

[23] Polar UV images covering the dawnside and the duskside sections of the polar cap were available in 34 cases of all 55 events. Table 2 shows the distribution of polar emissions at times of lobe cells on either the morningside (m) or the eveningside (e) of the polar cap. Here "TPA" corresponds to transpolar auroral emissions or Sun-aligned signatures not visibly connected to the dayside auroral oval, and "DPE" refers to diffuse polar emissions. Seven cases indicated the presence of a clear transpolar feature, or a Sun-aligned signature emanating from the nightside oval, either on the dawnside or the duskside in correlation with lobe convection signatures. Seven images showed only diffuse emissions in the polar cap, either on the dawnside or the duskside. Seven cases showed a diffuse emission region simultaneously with a Sun-aligned feature on the polar cap border (see, e.g., Figure 8). The remaining thirteen cases showed neither diffuse emissions, nor structured Sun-aligned arcs in Polar UVI. We note also that "TPA" signatures seemed to be more common on the duskside than the dawnside, although the number of dawnside events with Polar UVI data were somewhat lower.

[24] The distribution of the provisional *AE* indices versus IMF B_z and B_y for all 55 events are shown in Figure 12. The *AE* indices are averaged over the FAST time intervals above 60° ILat (see Figure 10). We observe that the stronger southward the average IMF B_z component is (Figure 12, top), the larger the resulting average *AE* index. This is the expected half-wave rectifier response of geomagnetic activity to the solar wind [e.g., *Crooker*, 1980]. What these distributions further indicate is the importance of the IMF B_y component (Figure 12, bottom) for substorm-like conditions in connection with these lobe convection events, if we assume that the *AE* index is a reliable measure of substorm activity. An increased IMF B_y appears to correspond to an increased *AE* index. The corresponding *AE* versus IMF B_x distribution did not indicate a similar dependence. The mean distribution averages for the positive and the negative IMF B_y subsets are marked by two crosses, respectively, at (B_y, *AE*) = (4.4, 180) nT and (B_y, *AE*) = (−2.5, 226) nT. The average *AE* indices thus indicate more active times than the 50 nT levels reported by *Hones et al.* [1989]. This may explain why diffuse UV emissions were detected on either the morningside or the eveningside. It may also be that the actual location of the lobe reconnection merging sites provides a global instability in the tail lobe that initiates a substorm. Another feature that may be linked to the IMF B_y dependent "TPA" signatures and the substorm-like conditions is the presence of an auroral oval intensification "spot" that appeared in the premidnight and/or the 1500 MLT region in ~59% of all 34 cases with UVI coverage. The premidnight 2000–2400 MLT sector spot turned out to be more common in this data set (13 cases) than the 1500 MLT spot, which either occurred alone (3 cases) or together with the premidnight spot (4 cases). We will return to this issue in the following section.

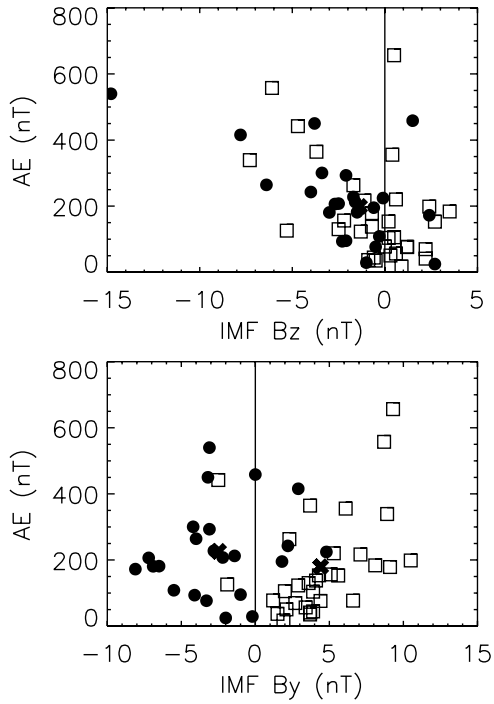

Figure 12. Average provisional *AE* indices versus IMF B_z (top) and B_y (bottom) for 23 morningside events (dot) and 32 eveningside events (square). Black crosses represent the following distribution averages: (B_z, *AE*) = (−1.4, 199) nT, (B_y, *AE*) = (−2.5, 226) nT, and (B_y, *AE*) = (4.4, 180) nT.

Table 2. Distribution of 34 Available High-Latitude Polar UV Emissions at Times of Morningside (m) and Eveningside (e) Lobe Cell Events[a]

emission	m	e
TPA	1	6
DPE	4	3
TPA and DPE	1	6
No TPA, no DPE	9	4

[a]"TPA" refers to clear transpolar auroral emissions as well as Sun-aligned signatures that does not connect across the polar cap to the dayside at this resolution. "DPE" corresponds to diffuse polar emissions.

3. Discussion

[25] As seen by the examples presented here and elsewhere [e.g., *Frank et al.*, 1986; *Cumnock et al.*, 1997; *Chang et al.*, 1998], large-scale particle precipitation and convection signatures in the region poleward of the auroral oval seem to be intimately correlated with each other and related to the IMF B_y component. A similar outline of IMF B_y-dependent global convection and auroral configuration was proposed by *Jankowska et al.* [1990] using Viking auroral images (see their Figures 3 and 4). However, they did not mention the persistence of this pattern for southward IMF B_z and only one pass of Viking electric field data was used to corroborate the suggested ionospheric convection signatures.

[26] Most frequently, we observed two types of precipitation as indicated by Polar UVI. Sometimes, the particle precipitation causes diffuse UV emissions reminiscent of the

so-called "horse collar aurora" [*Hones et al.*, 1989], though present only on that side of the polar cap coinciding with lobe cell convection. Occasionally, the boundary between the diffuse emission region and the polar cap proper show intensifications that develop into transpolar-like features (Figure 8). At other times, the emissions indicate a clear transpolar arc without the intermediate diffuse emission region (Figure 1a) or a "finger-like" protrusion into the polar cap (Figure 4a) that may or may not extend across to the dayside auroral oval below the UVI emission threshold as suggested by the sunward convection signature observed sunward of it. Low-altitude FAST and Polar UVI observations in the Northern Hemisphere thus imply an IMF B_y-dependent connection between lobe cell convection and particle precipitation, either with transpolar arcs or diffuse-like emissions reminiscent of the morningside or eveningside part of the horse-collar aurora [*Hones et al.*, 1989]. As Table 2 suggests, there is either diffuse or structured emissions present in ~62% of the examined 34 cases, while ~38% of the cases show no emissions in conjunction with ionospheric lobe cell signatures. Although the statistical data set is rather small, there seems to exist an asymmetric distribution of these emissions with structured transpolar-like emissions being more likely to occur on the duskside than the dawnside and more cases with no emissions on the dawnside than the duskside.

[27] *Newell and Meng* [1995] suggested that transpolar arcs occur exclusively for southward turnings of the IMF B_z after a prolonged period of northward IMF. It seems, however, that also northward turnings may trigger the development of such features in UVI data, as noted in our case study. We note that any large-scale shift in the direction of IMF B_z for a steady positive or negative IMF B_y would cause large $|B_y/B_z|$ ratios and result in IMF clock angles $|\theta|$ in the 45° to 135° range.

[28] As indicated by Polar UVI and the provisional *AE* versus IMF distributions (Figure 12) there seems to be a connection between lobe convection and substorm-like conditions. Although the coexistence of substorms and UV emissions indicating transpolar aurora and/or diffuse precipitation seems contradictory, observations of such situations have indeed been reported [e.g., *Henderson et al.*, 1996; *Weygand et al.*, 2001] and at times even occurred during IMF $B_z < 0$ conditions [*Murphree et al.*, 1994]. Indications of substorm-like activity in the auroral oval region appeared most clearly in Polar UVI as localized intensification "spots" in the premidnight and/or the 1500 MLT region. It has been noted that these "spots" are somehow related to transpolar arcs [e.g., *Murphree et al.*, 1987; *Liou et al.*, 1999]. When FAST went through the 1500 MLT spot on passes 3553 and 3585 (not shown), electron precipitation appeared as a large-scale ~1800 km wide inverted V-like feature in energy versus time spectra located primarily on sunward convection with peak energy fluxes above 1 keV located at the convection reversal boundary. A similar electron signature, though weaker, was observed for a dominant IMF $B_y < 0$ case on the dawnside for orbit 6301 (see Figure 5b) but did not appear as clearly, however, as did the duskside 1500 MLT spot in the Polar UVI (see Figure 4b). *Siscoe et al.* [2001b], in applying the *White et al.* [1998] MHD model, proposed a solution for the appearence of the "1500 MLT spot" in the crescent shaped convection cell present on the opposite side of the lobe cell as due to particles being accelerated through the resulting global parallel electric field, derived from Faraday's law used in the MHD model. This process would seem to explain the presence of the 1500 MLT spot in the Northern Hemisphere primarily for IMF $B_y < 0$ conditions [e.g., *Shue et al.*, 2001], but does not fully solve the problem of the appearing premidnight spot in the 2000–2400 MLT sector.

[29] Reconnection between the magnetic fields of the magnetosheath and the lobe and/or plasma sheet is a possible candidate for the low-altitude observation of sunward convection as suggested by the strong dependence on the IMF, by recent in situ plasma observations [e.g., *Raeder et al.*, 2000; *Avanov et al.*, 2001; *Popescu et al.*, 2001; *Maynard et al.*, 2001], and by modeling results from both the MHD [e.g., *Crooker et al.*, 1998; *White et al.*, 1998; *Raeder et al.*, 2000] and the kinetic perspectives [*Nishikawa*, 1998]. In tracing field lines from the ionospheric sunward lobe convection regions using the T01 model [*Tsyganenko*, 2002], it is confirmed that these regions map to the dawnside (duskside) tail lobe flanks for IMF $B_y < 0$ ($B_y > 0$). The merging geometry suggested by the statistical results in Figure 11 and the T01 model tracing results indicate a preferential region on the flank magnetopause that is expected to coincide with the magnetospheric sash [e.g., *Siscoe et al.*, 2001a]. Regarding the use of the Tsyganenko T01 model, it should be noted that it is not a dynamic MHD model and it is uncertain whether it may correctly represent the conditions during the suggested lobe reconnection presented here. It should primarily be viewed as providing the general directions of the geomagnetic field possibly prevailing prior to merging and that these regions (see Figure 9) may be involved in the sunward convection of plasma driven by lobe reconnection. The singularities reported in the MHD mapping between the tail lobe and the ionosphere during lobe reconnection [*Raeder et al.*, 2000] is therefore not expected to appear using the T01 model.

[30] We note further that at any given time, the IMF most often lies near the ecliptic plane. The IMF clock angle $|\theta|$ is thus expected to most often lie in the 45° to 135° range for any randomly selected set of time intervals. This implies that this angle alone does not necessarily predict lobe reconnection. Other factors that may be of importance to increase the probability of magnetic merging on the tail lobe flanks are low Alfvén Mach numbers and low β values in the adjacent magnetosheath [e.g., *Hughes*, 1995; *Crooker et al.*, 1998], which seems to have been the case for the events presented in this study.

[31] The dawn-dusk asymmetry of polar rain intensity across the polar cap observed here and reported elsewhere [e.g., *Meng et al.*, 1977] may partly be explained by IMF B_y-dependent lobe reconnection as was suggested by *Shirai et al.* [1998], who advanced the idea that the earthward polar rain flux may get disrupted at an X line in the tail.

[32] We propose the following hypothesis, the schematic of which can be found in Figure 10 of *Eriksson et al.* [2002], to explain the observed coexistence of IMF B_y-dependent lobe convection and high-latitude precipitation. The B_y component of the IMF is expected to produce a rotation of the magnetotail that shifts the boundary plasma sheet to higher latitudes on the duskside (dawnside) in the Northern Hemisphere and on the dawnside (duskside) in the

Southern Hemisphere for positive (negative) B_y [*Siscoe and Sanchez*, 1987; *Cowley et al.*, 1991]. As indicated by MHD models and the superposition of magnetosheath and geomagnetic fields in vacuum for these IMF B_y conditions [*Luhmann et al.*, 1984; *White et al.*, 1998; *Siscoe et al.*, 2001a; *Maynard et al.*, 2001], lobe reconnection may occur where these magnetic fields are antiparallel if conditions such as low magnetosheath Alfvén Mach number and low plasma β value are fulfilled. Taken together, these two processes could explain the presence of plasma sheet-like and magnetosheath-like populations in regions of sunward convection, the dawn-dusk asymmetric disruption of polar rain [*Meng et al.*, 1977; *Shirai et al.*, 1998], and may initiate an instability in the tail as the convection flow is redirected that promotes the release of stored tail magnetic field energy in a substorm. As the magnetosheath magnetic field changes direction, the antiparallel merging site would move, resulting in a motion or disruption of the ionospheric lobe cell, and thus a relocation of the region of sheared convection velocity [e.g., *Lassen*, 1979; *Jankowska et al.*, 1990] and the motion or fading of transpolar auroral emissions. Assume that the distinct transpolar arc is connected to the lobe reconnection site by a pair of field-aligned currents poleward of the region 1 current [*Eriksson et al.*, 2002] and that the diffuse emissions between the arc and the oval are found in the tilted boundary plasma sheet near the merging site. A change in the IMF B_y direction from positive to negative would then separate the transpolar arc from the diffuse emissions on the duskside as the tail relaxes to a less tilted dusk-type configuration, or even changes its tilt angle to a dawn-type configuration, and the merging site moves toward the dawnside.

[33] The question is whether IMF B_y-dependent lobe reconnection may result in sunward convection at ionospheric altitudes, or rather whether the magnetosheath Alfvén Mach number is low enough to sustain a quasi-steady reconnection site with the accelerated flow of plasma being able to overcome the momentum of the antisunward flows. *Fuselier et al.* [2000] invoked a plasma depletion layer along the magnetopause to explain the apparent long-term stability of a high-latitude reconnection site as observed by the Polar spacecraft in a region often deemed as super-Alfvénic [*Spreiter and Stahara*, 1985]. The question of sub-Alfvénic versus super-Alfvénic flow regimes along the magnetopause and the stability of the reconnection site has been treated in a few other publications [e.g., *La Belle-Hamer et al.*, 1995; *Rodger et al.*, 2000]. Adopting the antiparallel merging hypothesis to study the magnetopause locations of transient and quasi-steady state reconnection at the magnetopause, *Rodger et al.* [2000] concluded that the condition of fields being within 10° of pure antiparallel alignment is met within a sub-Alfvénic region at the dusk (dawn) high-altitude Northern Hemispheric flanks for an IMF with equal magnitudes of a positive (negative) B_y and a negative B_z. The opposite dawn-dusk dependence on IMF B_y is predicted in the Southern Hemisphere. These sub-Alfvénic regions are likely to coincide with the magnetic field minima domains along the magnetopause referred to as the magnetospheric sash. However, the YZ_{GSM}-plane projection of the magnetopause boundary between sub- and super-Alfvénic flow regions that Rodger et al. derived is based on the theoretical Spreiter and Stahara gasdynamic model and should increase in radial dimension, i.e., move tailward, by applying the reasoning of *Fuselier et al.* [2000].

4. Summary and Conclusions

[34] We have examined the global auroral precipitation pattern using Polar UVI data in connection with 34 events of lobe cell convection signatures detected in electric and magnetic field data from the FAST satellite. As a result of this study, we make the following conclusions.

[35] 1. A total of 21 events of all 34 concurrent FAST and Polar UVI conjunctions showed that the IMF B_y-dependent sunward convection region of the lobe cell coincided with either a transpolar or Sun-aligned arc feature emanating from the nightside auroral oval, diffuse-appearing emissions, or both. These diffuse-like emission regions resemble the dawnside or the duskside part of the so-called horse-collar auroral pattern reported by *Hones et al.* [1989]. The remaining 13 events showed neither diffuse nor structured UV emissions. This result generally supports the proposed B_y-dependent convection and auroral distribution pattern by *Jankowska et al.* [1990] with dawnside features for $B_y < 0$ and duskside features for $B_y > 0$ in the Northern Hemisphere based on the *Burch et al.* [1985] convection picture.

[36] 2. The suggested origin of low-altitude particle precipitation is most often plasma sheet-like (33 out of 55 cases) and in fewer cases magnetosheath-like (16 out of 55). Six events did not show any particle precipitation. This result supports the proposed IMF B_y-dependent reconnection and magnetotail rotation model about the Sun-Earth line [*Meng*, 1981; *Siscoe and Sanchez*, 1987; *Jankowska et al.*, 1990; *Cowley et al.*, 1991; *Kullen*, 2000; *Eriksson et al.*, 2002] that brings the boundary plasma sheet to higher latitudes for transpolar auroral formation.

[37] 3. For all the 55 examined cases, it seemed that a majority of cases occurred during disturbed geomagnetic conditions as indicated by the provisional *AL* and *AE* indices. Furthermore, a stronger IMF B_y is reflected in a stronger *AE* index. Whether or not some or all of these are indeed substorm periods is impossible to conclude using these data sets. Although the coexisting signatures of transpolar arcs and diffuse emissions during substorms seem contradictory, reports have been published on their coexistence [e.g., *Murphree et al.*, 1994; *Henderson et al.*, 1996; *Weygand et al.*, 2001].

[38] 4. A premidnight and/or 1500 MLT injection spot [e.g., *Murphree et al.*, 1987; *Liou et al.*, 1999] appeared in ~59% of all cases with UVI coverage and could partly be explained by global field-aligned potential drops in connection with these lobe reconnection events [*Siscoe et al.*, 2001b].

[39] 5. The IMF B_y-dependent asymmetric intensity distribution of polar rain across the polar cap [*Meng et al.*, 1977] is again evident in this study, with 24 of all 55 cases showing clear intensity minima near the lobe cell convection reversal. *Shirai et al.* [1998] suggested that the earthward polar rain fluxes may be disrupted at an X line in the tail. It seems from our results that a B_y-dependent lobe reconnection site may act as such an obstacle.

[40] 6. We have presented one case of a transpolar arc that probably formed about two hours prior to the time interval

shown here, when the time-shifted IMF data from the Wind spacecraft suggested a northward turning of the IMF B_z. This one example shows that transpolar arcs do not form exclusively for southward turnings of the IMF B_z as *Newell and Meng* [1995] have claimed and clearly indicates the importance of the B_y component for transpolar arc formation. The same conclusions can be drawn from the existence of such arcs during substorm conditions, if we assume that the formation of transpolar arcs occur for B_y (rather than B_z) dominant situations.

[41] Theory, MHD model predictions, and recent in situ data show sunward convection in the polar cap. Although the coupling efficiency between the high-altitude lobe region and the ionosphere is an unknown parameter at the present, there are compelling evidence in low-altitude satellite data [e.g., *Burch et al.*, 1985; *Coley et al.*, 1987; *Lu et al.*, 1994; *Matsuoka et al.*, 1996; *Eriksson et al.*, 2002], ground magnetometer data [e.g., *Maezawa*, 1976], and remote sensing ground equipment such as optical and radar observations [e.g., *Øieroset et al.*, 1997; *Sandholt et al.*, 2001, 2003] in support of lobe reconnection and subsequent lobe cell convection in the polar cap. Recent high-altitude in situ observations by, e.g., *Raeder et al.* [2000] and *Maynard et al.* [2001] seem to verify the connection between high-altitude regions of IMF B_y dependent lobe reconnection along the flank magnetopause with the low-altitude observations reported here, as suggested by the mapping of field lines from the ionospheric sunward lobe convection regions to the tail lobe flanks using the *Tsyganenko* [2002] T01 model. However, more evidence is needed from in situ lobe observations, such as the Cluster II mission, to verify whether the hypothetical processes proposed here between high and low altitudes indeed occurs.

[42] **Acknowledgments.** The first author would like to thank Per Even Sandholt for helpful discussions and comments. We are also thankful to the World Data Center for Geomagnetism in Kyoto, Japan, for providing auroral electrojet indices. This research was conducted under NASA grant NAG5-3596.

[43] Arthur Richmond thanks Joachim Raeder and another reviewer for their assistance in evaluating this article.

References

Avanov, L. A., V. N. Smirnov, J. H. Waite Jr., S. A. Fuselier, and O. L. Vaisberg, High-latitude magnetic reconnection in sub-Alfvénic flow: Interball Tail observations on May 29 1996, *J. Geophys. Res.*, *106*, 29,491–29,502, 2001.

Burch, J. L., P. H. Reiff, J. D. Menietti, R. A. Heelis, W. B. Hanson, S. D. Shawhan, E. G. Shelley, M. Sugiura, D. R. Weimer, and J. D. Winningham, IMF B_y-dependent plasma flow and Birkeland currents in the dayside magnetosphere: 1. Dynamics Explorer observations, *J. Geophys. Res.*, *90*, 1577–1593, 1985.

Carlson, C. W., R. F. Pfaff, and J. G. Watzin, The Fast Auroral SnapshoT (FAST) mission, *Geophys. Res. Lett.*, *25*, 2013–2016, 1998.

Chang, S.-W., et al., A comparison of a model for the theta aurora with observations from Polar, Wind, and SuperDARN, *J. Geophys. Res.*, *103*, 17,367–17,390, 1998.

Coley, W. R., R. A. Heelis, W. B. Hanson, P. H. Reiff, J. R. Sharber, and J. D. Winningham, Ionospheric convection signatures and magnetic field topology, *J. Geophys. Res.*, *92*, 12,352–12,364, 1987.

Cowley, S. W. H., J. P. Morelli, and M. Lockwood, Dependence of convective flows and particle precipitation in the high-latitude dayside ionosphere on the *X* and *Y* components of the interplanetary magnetic field, *J. Geophys. Res.*, *96*, 5557–5564, 1991.

Crooker, N. U., Dayside merging and cusp geometry, *J. Geophys. Res.*, *84*, 951–959, 1979.

Crooker, N. U., The half-wave rectifier response of the magnetosphere and antiparallel merging, *J. Geophys. Res.*, *85*, 575–578, 1980.

Crooker, N. U., Reverse convection, *J. Geophys. Res.*, *97*, 19,363–19,372, 1992.

Crooker, N. U., G. L. Siscoe, and F. R. Toffoletto, A tangent subsolar merging line, *J. Geophys. Res.*, *95*, 3787–3793, 1990.

Crooker, N. U., J. G. Lyon, and J. A. Fedder, MHD model merging with IMF B_y: Lobe cells, sunward polar cap convection, and overdraped lobes, *J. Geophys. Res.*, *103*, 9143–9151, 1998.

Cumnock, J. A., J. R. Sharber, R. A. Heelis, M. R. Hairston, and J. D. Craven, Evolution of the global aurora during positive IMF B_z and varying IMF B_y conditions, *J. Geophys. Res.*, *102*, 17,489–17,497, 1997.

Cumnock, J. A., J. R. Sharber, R. A. Heelis, L. G. Blomberg, G. A. Germany, J. F. Spann, and W. R. Coley, Interplanetary magnetic field control of theta aurora development, *J. Geophys. Res.*, *107*(A7), 1108, doi:10.1029/2001JA009126, 2002.

Dungey, J. W., The structure of the exosphere, or adventures in velocity space, in *Geophysics: The Earth's Environment*, edited by C. DeWitt, J. Hieblot, and A. Lebeau, pp. 503–550, Gordon and Breach, Newark, N. J., 1963.

Eriksson, S., J. W. Bonnell, L. G. Blomberg, R. E. Ergun, G. T. Marklund, and C. W. Carlson, Lobe cell convection and field-aligned currents poleward of the region 1 current system, *J. Geophys. Res.*, *107*(A8), 1185, doi:10.1029/2001JA005041, 2002.

Frank, L. A., J. D. Craven, J. L. Burch, and J. D. Winningham, Polar views of the Earth's aurora with Dynamics Explorer, *Geophys. Res. Lett.*, *9*, 1001–1004, 1982.

Frank, L. A., et al., The theta aurora, *J. Geophys. Res.*, *91*, 3177–3224, 1986.

Fuselier, S. A., S. M. Petrinec, and K. J. Trattner, Stability of the high-latitude reconnection site for steady northward IMF, *Geophys. Res. Lett.*, *27*, 473–476, 2000.

Gonzalez, W. D., and F. S. Mozer, A quantitative model for the potential resulting from reconnection with an arbitrary interplanetary magnetic field, *J. Geophys. Res.*, *79*, 4186–4194, 1974.

Gosling, J. T., M. F. Thomsen, S. J. Bame, R. C. Elphic, and C. T. Russell, Plasma flow reversals at the dayside magnetopause and the origin of asymmetric polar cap convection, *J. Geophys. Res.*, *95*, 8073–8084, 1990.

Gosling, J. T., M. F. Thomsen, S. J. Bame, R. C. Elphic, and C. T. Russell, Observations of reconnection of interplanetary and lobe magnetic field lines at the high-latitude magnetopause, *J. Geophys. Res.*, *96*, 14,097–14,106, 1991.

Henderson, M. G., J. S. Murphree, and J. M. Weygand, Observations of auroral substorms occurring together with preexisting "quiet time" auroral patterns, *J. Geophys. Res.*, *101*, 24,621–24,640, 1996.

Hones, E. W., Jr., J. D. Craven, L. A. Frank, D. S. Evans, and P. T. Newell, The horse-collar aurora: A frequent pattern of the aurora in quiet times, *Geophys. Res. Lett.*, *16*, 37–40, 1989.

Huang, C. Y., L. A. Frank, W. K. Peterson, D. J. Williams, W. Lennartsson, D. G. Mitchell, R. C. Elphic, and C. T. Russell, Filamentary structures in the magnetotail lobes, *J. Geophys. Res.*, *92*, 2349–2363, 1987.

Hughes, W. J., The magnetopause, magnetotail, and magnetic reconnection, in *Introduction to Space Physics*, edited by M. G. Kivelson and C. T. Russell, pp. 227–287, Cambridge Univ. Press, New York, 1995.

Jankowska, K., R. D. Elphinstone, J. S. Murphree, L. L. Cogger, D. Hearn, and G. Marklund, The configuration of the auroral distribution for interplanetary magnetic field B_z northward: 2. Ionospheric convection consistent with Viking observations, *J. Geophys. Res.*, *95*, 5805–5816, 1990.

Kessel, R. L., S.-H. Chen, J. L. Green, S. F. Fung, S. A. Boardsen, L. C. Tan, T. E. Eastman, J. D. Craven, and L. A. Frank, Evidence of high-latitude reconnection during northward IMF: Hawkeye observations, *Geophys. Res. Lett.*, *23*, 583–586, 1996.

Kullen, A., The connection between transpolar arcs and magnetotail rotation, *Geophys. Res. Lett.*, *27*, 73–76, 2000.

La Belle-Hamer, A. L., A. Otto, and L. C. Lee, Magnetic reconnection in the presence of sheared flow and density asymmetry: Application to the Earth's magnetopause, *J. Geophys. Res.*, *100*, 11,875–11,889, 1995.

Lassen, K., The quiet-time pattern of auroral arcs as a consequence of magnetospheric convection, *Geophys. Res. Lett.*, *6*, 777–780, 1979.

Liou, K., P. T. Newell, C.-I. Meng, T. Sotirelis, M. Brittnacher, and G. Parks, Source region of 1500 MLT auroral bright spots: Simultaneous Polar UV-images and DMSP particle data, *J. Geophys. Res.*, *104*, 24,587–24,602, 1999.

Lu, G., et al., Interhemispheric asymmetry of the high-latitude ionospheric convection pattern, *J. Geophys. Res.*, *99*, 6491–6510, 1994.

Luhmann, J. G., R. J. Walker, C. T. Russell, N. U. Crooker, J. R. Spreiter, and S. S. Stahara, Patterns of potential magnetic field merging sites on the dayside magnetopause, *J. Geophys. Res.*, *89*, 1739–1742, 1984.

Maezawa, K., Magnetospheric convection induced by the positive and negative *Z* components of the interplanetary magnetic field: Quantitative analysis using polar cap magnetic records, *J. Geophys. Res.*, *81*, 2289–2303, 1976.

Makita, K., C.-I. Meng, and S.-I. Akasofu, Transpolar auroras, their particle precipitation, and IMF B_y component, *J. Geophys. Res.*, *96*, 14,085–14,095, 1991.

Marcucci, M. F., et al., Evidence for interplanetary magnetic field B_y controlled large-scale reconnection at the dayside magnetopause, *J. Geophys. Res.*, *105*, 27,497–27,507, 2000.

Matsuoka, A., K. Tsuruda, H. Hayakawa, T. Mukai, and A. Nishida, Electric field structure and ion precipitation in the polar region associated with northward interplanetary magnetic field, *J. Geophys. Res.*, *101*, 10,711–10,736, 1996.

Maynard, N. C., et al., Observation of the magnetospheric "sash" and its implications relative to the solar-wind/magnetospheric coupling: A multi-satellite event analysis, *J. Geophys. Res.*, *106*, 6097–6122, 2001.

Meng, C.-I., Polar cap arcs and the plasma sheet, *Geophys. Res. Lett.*, *8*, 273–276, 1981.

Meng, C.-I., S.-I. Akasofu, and K. A. Anderson, Dawn-dusk gradient of the precipitation of low-energy electrons over the polar cap and its relation to the interplanetary magnetic field, *J. Geophys. Res.*, *82*, 5271–5275, 1977.

Murphree, J. S., L. L. Cogger, C. D. Anger, D. D. Wallis, and G. G. Shepherd, Oval intensifications associated with polar arcs, *Geophys. Res. Lett.*, *14*, 403–406, 1987.

Murphree, J. S., J. B. Austin, D. J. Hearn, L. L. Cogger, R. D. Elphinstone, and J. Woch, Satellite observations of polar arcs, *J. Atmos. Terr. Phys.*, *56*, 265–284, 1994.

Newell, P. T., and C.-I. Meng, Creation of theta-auroras: The isolation of plasma sheet fragments in the polar cap, *Science*, *270*, 1338–1341, 1995.

Newell, P. T., W. J. Burke, E. R. Sanchez, C.-I. Meng, M. E. Greenspan, and C. R. Clauer, The low-latitude boundary layer and the boundary plasma sheet at low altitude: Prenoon precipitation regions and convection reversal boundaries, *J. Geophys. Res.*, *96*, 21,013–21,023, 1991.

Nishikawa, K.-I., Particle entry through reconnection grooves in the magnetopause with a dawnward IMF as simulated by a 3-D EM particle code, *Geophys. Res. Lett.*, *25*, 1609–1612, 1998.

Ohtani, S., et al., Four large-scale field-aligned current systems in the dayside high-latitude region, *J. Geophys. Res.*, *100*, 137–153, 1995.

Øieroset, M., P. E. Sandholt, W. F. Denig, and S. W. H. Cowley, Northward interplanetary magnetic field cusp aurora and high-latitude magnetopause reconnection, *J. Geophys. Res.*, *102*, 11,349–11,362, 1997.

Onsager, T. G., J. D. Scudder, M. Lockwood, and C. T. Russell, Reconnection at the high-latitude magnetopause during northward interplanetary magnetic field conditions, *J. Geophys. Res.*, *106*, 25,467–25,488, 2001.

Peterson, W. K., and E. G. Shelley, Origin of the plasma in a cross-polar cap auroral feature, *J. Geophys. Res.*, *89*, 6729–6736, 1984.

Popescu, D., J.-A. Sauvaud, A. Fedorov, E. Budnik, H. Stenuit, and T. Moreau, Evidence for a sunward flowing plasma layer adjacent to the tail high-latitude magnetopause during dawnward directed interplanetary field, *J. Geophys. Res.*, *106*, 29,479–29,489, 2001.

Raeder, J., O. Vaisberg, V. Smirnov, and L. Avanov, Reconnection driven lobe convection: Interball tail probe observations and global simulations, *J. Atmos. Terr. Phys.*, *62*, 833–849, 2000.

Rodger, A. S., I. J. Coleman, and M. Pinnock, Some comments on transient and steady-state reconnection at the dayside magnetopause, *Geophys. Res. Lett.*, *27*, 1359–1362, 2000.

Russell, C. T., The configuration of the magnetosphere, in *Critical Problems of Magnetospheric Physics*, edited by E. R. Dyer Jr., pp. 1–16, Natl. Acad. of Sci., Washington, D. C., 1972.

Sandholt, P.-E., C. J. Farrugia, S. W. H. Cowley, and M. Lester, Dayside auroral bifurcation sequence during B_y-dominated interplanetary magnetic field: Relationship with merging and lobe convection cells, *J. Geophys. Res.*, *106*, 15,429–15,444, 2001.

Sandholt, P.-E., J. Moen, C. J. Farrugia, S. W. H. Cowley, M. Lester, S. E. Milan, C. Valladares, W. F. Denig, and S. Eriksson, Multi-site observations of the association between aurora and plasma convection in the cusp/polar cap during a southeastward ($B_y \sim |B_z|$) IMF orientation, *Ann. Geophys.*, *21*, 539–558, 2003.

Shirai, H., K. Maezawa, M. Fujimoto, T. Mukai, T. Yamamoto, Y. Saito, and S. Kokubun, Entry process of low-energy electrons into the magnetosphere along open field lines: Polar rain electrons as field line tracers, *J. Geophys. Res.*, *103*, 4379–4390, 1998.

Shue, J.-H., P. T. Newell, K. Liou, and C.-I. Meng, Influence of interplanetary magnetic field on global auroral patterns, *J. Geophys. Res.*, *106*, 5913–5926, 2001.

Siscoe, G. L., and E. Sanchez, An MHD model for the complete open magnetotail boundary, *J. Geophys. Res.*, *92*, 7405–7412, 1987.

Siscoe, G. L., G. M. Erickson, B. U. Ö. Sonnerup, N. C. Maynard, K. D. Siebert, D. R. Weimer, and W. W. White, Magnetospheric sash dependence on IMF direction, *Geophys. Res. Lett.*, *28*, 1921–1924, 2001a.

Siscoe, G. L., G. M. Erickson, B. U. Ö. Sonnerup, N. C. Maynard, K. D. Siebert, D. R. Weimer, and W. W. White, Global role of $E_{\|}$ in magnetopause reconnection: An explicit demonstration, *J. Geophys. Res.*, *106*, 13,015–13,022, 2001b.

Spreiter, J. R., and S. S. Stahara, Magnetohydrodynamic and gasdynamic theories for planetary bow waves, in *Collisionless Shocks in the Heliosphere: Reviews of Current Research*, *Geophys. Monogr. Ser.*, vol. 35, edited by B. T. Tsurutani and R. G. Stone, pp. 85–107, AGU, Washington, D. C., 1985.

Torr, M. R., D. G. Torr, M. Zukic, R. B. Johnson, J. Ajello, P. Banks, K. Clark, K. Cole, C. Keffer, G. Parks, B. Tsurutani, and J. Spann, A far ultraviolet imager for the international solar-terrestrial physics mission, *Space Sci. Rev.*, *71*, 329–383, 1995.

Tsyganenko, N. A., A model of the near magnetosphere with a dawn-dusk asymmetry: 2. Parameterization and fitting to observations, *J. Geophys. Res.*, *107*(A8), 1176, doi:10.1029/2001JA000220, 2002.

Valladares, C. E., H. C. Carlson Jr., and K. Fukui, Interplanetary magnetic field dependency of stable sun-aligned polar cap arcs, *J. Geophys. Res.*, *99*, 6247–6272, 1994.

Weimer, D. R., An improved model of ionospheric electric potentials including substorm perturbations and application to the Geospace Environment Modeling November 24, 1996, event, *J. Geophys. Res.*, *106*, 407–416, 2001.

Weygand, J. M., J. S. Murphree, M. G. Henderson, and G. A. Enno, Simultaneous closed magnetic field line polar arcs and substorms, *J. Atmos. Terr. Phys.*, *63*, 643–655, 2001.

White, W. W., G. L. Siscoe, G. M. Erickson, Z. Kaymaz, N. C. Maynard, K. D. Siebert, B. U. Ö. Sonnerup, and D. R. Weimer, The magnetospheric sash and the cross-tail S, *Geophys. Res. Lett.*, *25*, 1605–1608, 1998.

Zhu, L., R. W. Schunk, and J. J. Sojka, Polar cap arcs: A review, *J. Atmos. Terr. Phys.*, *59*, 1087–1126, 1997.

J. W. Bonnell, C. W. Carlson, G. K. Parks, and Y.-K. Tung, Space Sciences Laboratory, University of California, Berkeley, CA 94720-7450, USA. (jbonnell@ssl.berkeley.edu)

R. E. Ergun, S. Eriksson, and Y.-J. Su, Laboratory for Atmospheric and Space Physics, University of Colorado, 1234 Innovation Drive, Boulder, CO 80303, USA. (eriksson@lasp.colorado.edu)

W. J. Peria, Department of Earth and Space Sciences, University of Washington, Box 351310, Seattle, WA 98195-1310, USA. (peria@geophys.washington.edu)

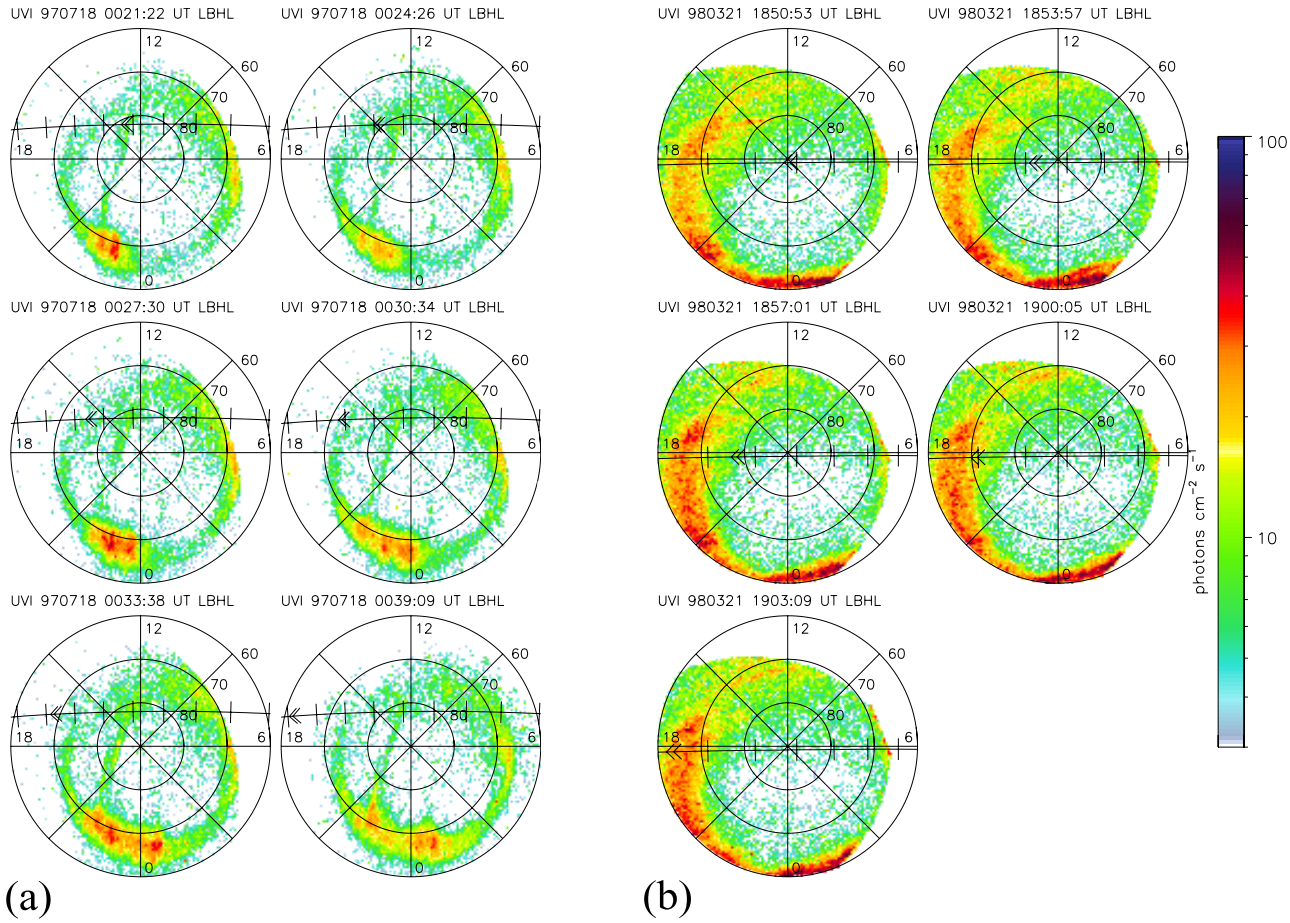

Figure 1. Polar UV images at the times of FAST orbits (a) 3575 and (b) 6246. FAST is moving from dawn to dusk as shown by the satellite track and the triangular marker that indicates the integration time interval for each Polar UV image.

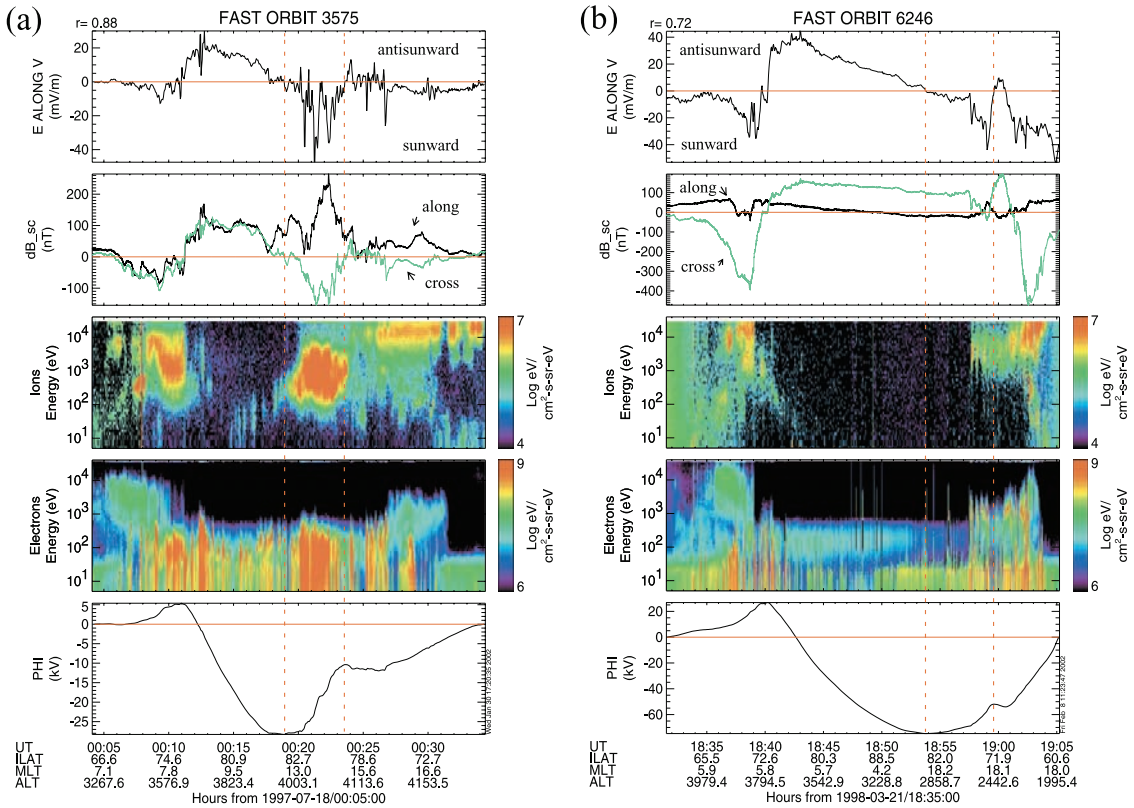

Figure 2. Two examples of lobe cell convection as observed by FAST on the duskside for positive IMF B_y, (a) FAST orbit 3575 and (b) FAST orbit 6246. The top two panels show the along-track electric field and the magnetic field (green is perpendicular, and black is along the direction of motion). The precipitating ion and electron energy flux versus energy and time are followed by the integrated electric field assuming a return to zero potential. Vertical dashed lines indicate the equatorward interval of sunward lobe convection.

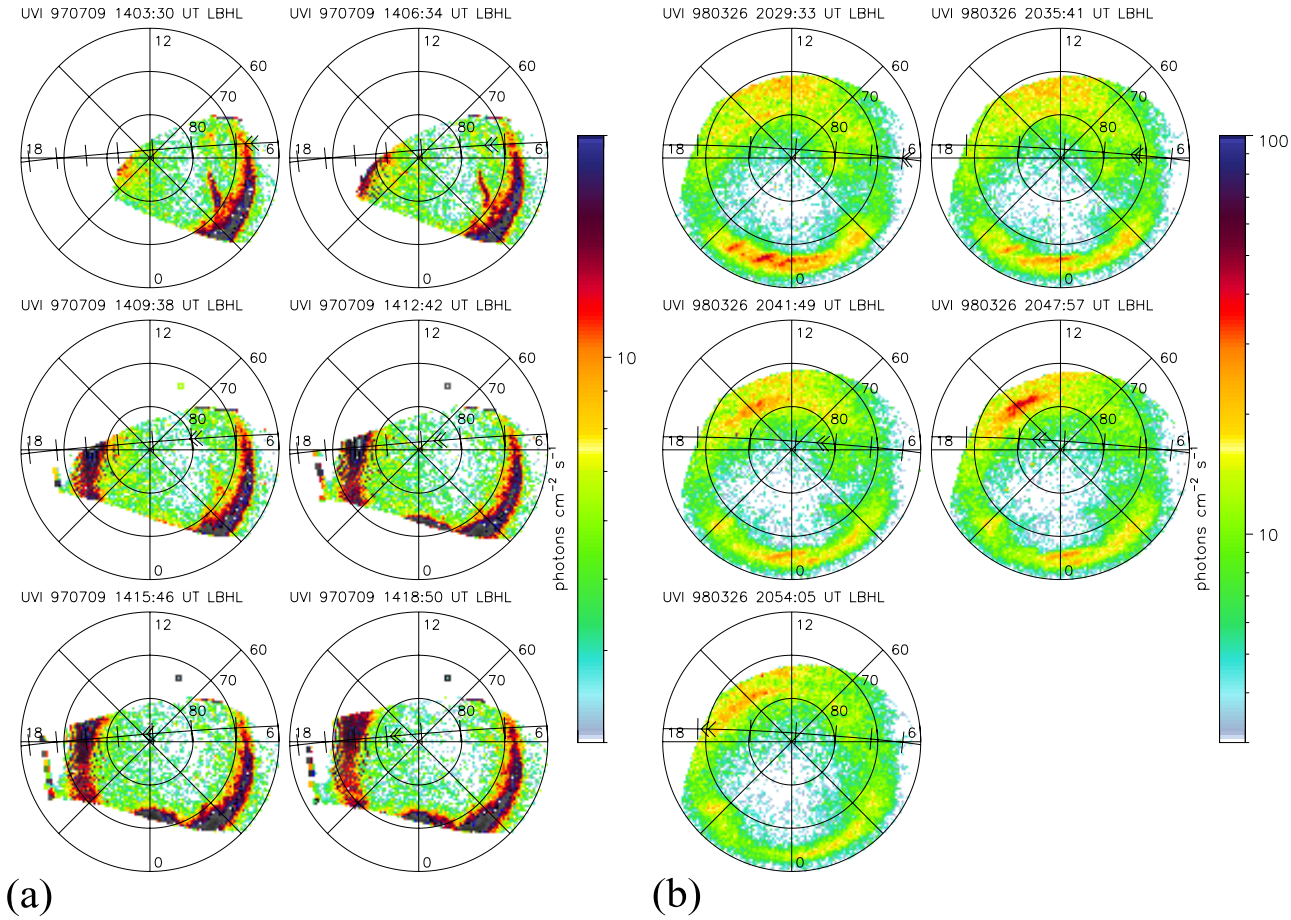

Figure 4. Polar UVI for FAST orbits (a) 3484 and (b) 6301. Same format as Figure 1. A different photon flux scale is used for the UV image on the left to enhance the transpolar arc feature on the dawnside of the polar cap.

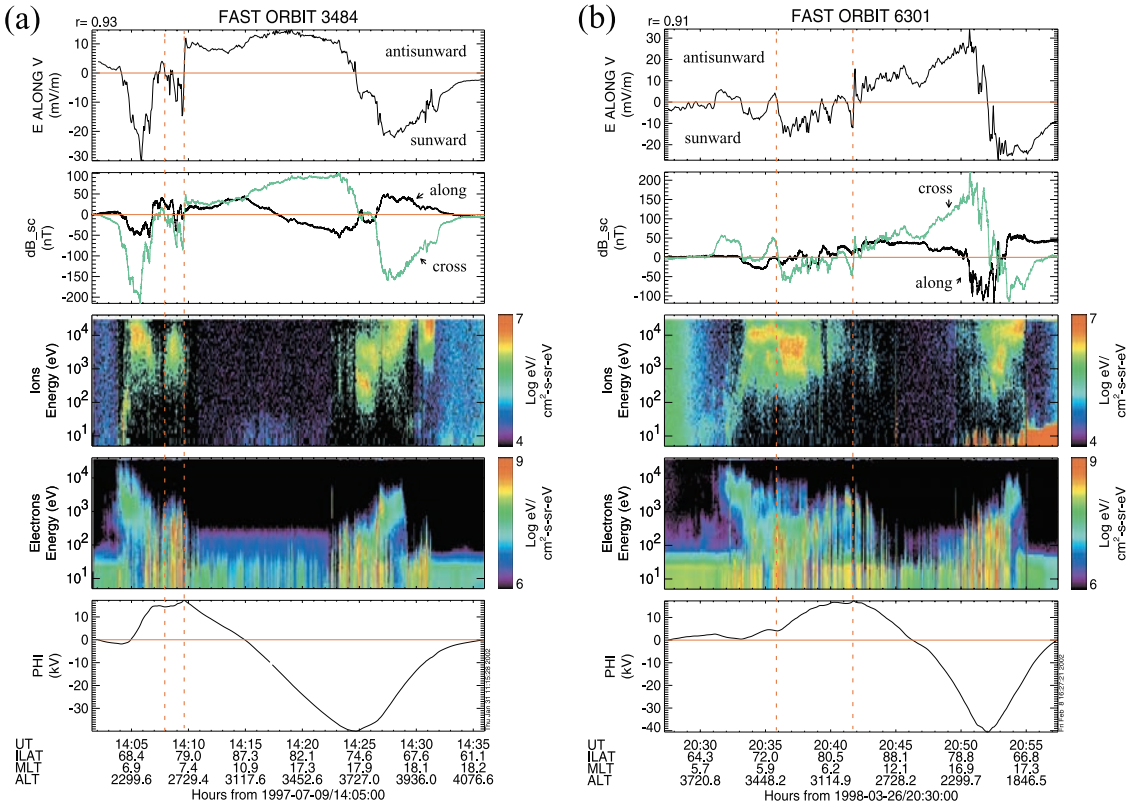

Figure 5. Two examples of lobe cell convection as observed by FAST on the dawnside for negative IMF B_y, FAST orbits (a) 3484 and (b) 6301. Same format as Figure 2.

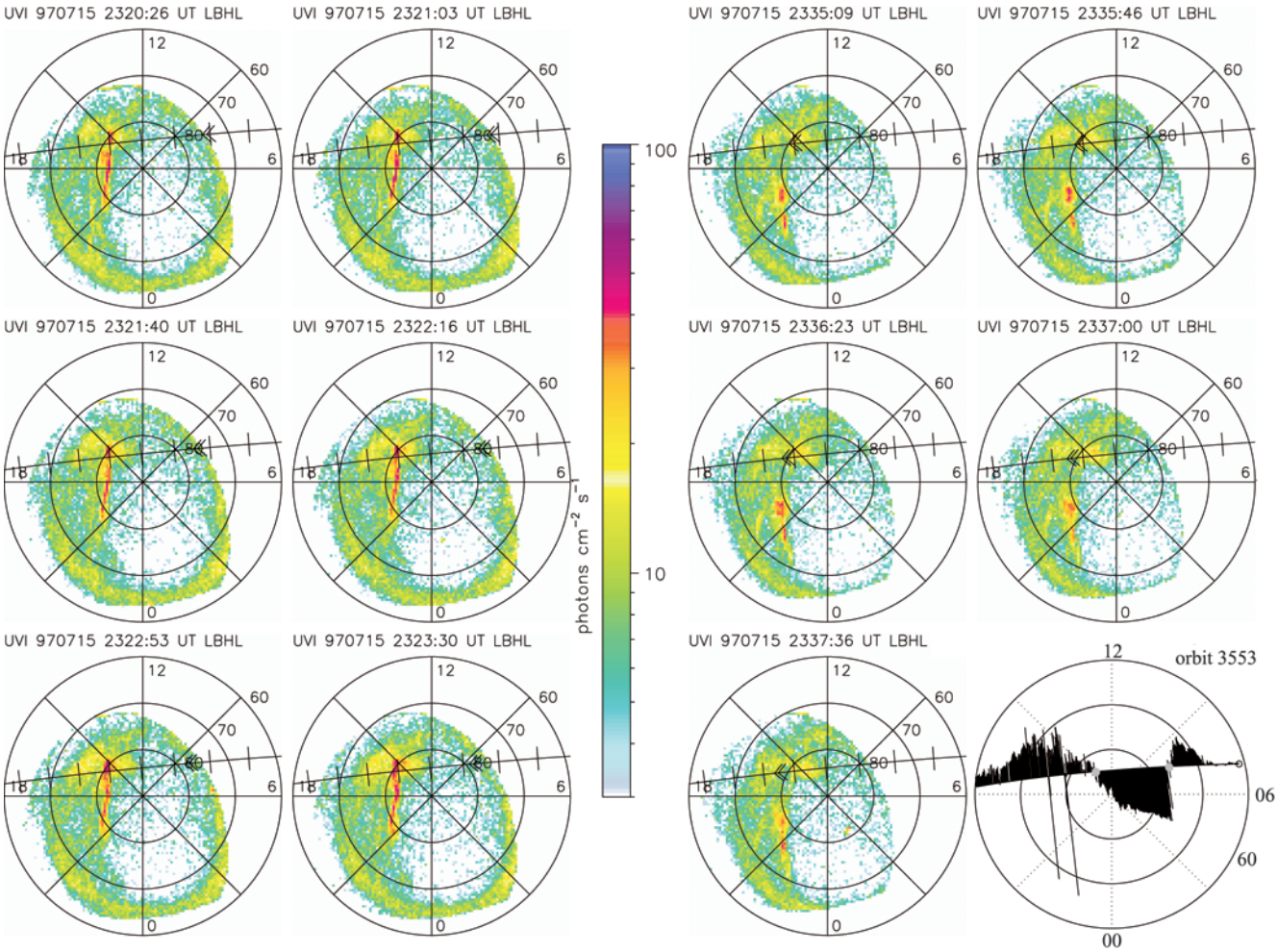

Figure 8. Polar UVI for FAST orbit 3553 from 1997-07-15 (read as 15 July 1997) 23:20:26 UT (top left) to 23:37:36 UT (bottom right). The corresponding $\vec{E} \times \vec{B}$ convection velocity is shown after the complete time sequence. Maximum shown drift velocity is 3.6 km/s. Note the transpolar-like auroral arc signature that develops on the border between the polar cap and the diffuse-appearing emissions on its equatorward side.